Advances in Colloid and Interface Science 252 (2018) 38–54

Contents lists available at ScienceDirect

Advances in Colloid and Interface Science

journal homepage: www.elsevier.com/locate/cis

Historical perspective

A review on suppression and utilization of the coffee-ring effect

Dileep Mampallil[a,*], Huseyin Burak Eral[b,*]

[a] Indian Institute of Science Education & Research Tirupati, Mangalam P. O., Tirupati-517507, India
[b] Process & Energy Department, 3ME Faculty, TU Delft, Leeghwaterstraat 39, 2628CB Delft, The Netherlands

ARTICLE INFO

Available online 2 January 2018

Keywords:
Coffee-ring effect
Evaporation
Droplets
Capillarity
Colloids

ABSTRACT

Evaporation of sessile droplets containing non-volatile solutes dispersed in a volatile solvent leaves behind ring-like solid stains. As the volatile species evaporates, pinning of the contact line gives rise to capillary flows that transport non-volatile solutes to the contact line. This phenomenon, called the coffee-ring effect, compromises the overall performance of industrially relevant manufacturing processes involving evaporation such as printing, biochemical analysis, manufacturing of nano-structured materials through colloidal and macromolecular patterning. Various approaches have been developed to suppress this phenomenon, which is otherwise difficult to avoid. The coffee-ring effect has also been leveraged to prepare new materials through convection induced assembly. This review underlines not only the strategies developed to suppress the coffee-ring effect but also sheds light on approaches to arrive at novel processes and materials. Working principles and applicability of these strategies are discussed together with a critical comparison.

Contents

* Corresponding authors at: Van't Hoff Laboratory for Physical and Colloid Chemistry, Debye Institute for Nanomaterials Science, Utrecht University, The Netherlands.
E-mail addresses: dileep.mampallil@iisertirupati.ac.in (D. Mampallil), h.b.eral@tudelft.nl (H.B. Eral).

https://doi.org/10.1016/j.cis.2017.12.008
0001-8686/

1. Introduction

A phenomenon omnipresent in nature, the evaporation of sessile droplets containing non-volatile solutes received a great deal of attention due to the richness of fundamental phenomenon it entails and the number of applied aspects connected to it [1–3].

One ubiquitous phenomenon occurring in the evaporation of sessile droplets containing non-volatile solutes is the contact line pinning and the formation of ring-like residues, called the coffee-stains or coffee-rings [1–5]. Understanding and controlling the process of solute deposition in the presence of coffee-ring effect (CRE) is important in manufacturing processes involving evaporation on surfaces including printing [6–9] and fabrication of ordered structures [24], functional nanomaterials [25,26] and colloidal crystals [27,28]. CRE also hampers the performance of commercial applications including fluorescent microarrays [10,11], matrix assisted laser desorption ionization (MALDI) spectrometry [12–15], and surface enhanced Raman spectroscopy (SERS) [16,17]. CRE has also implications in plasmonics [18], diagnostics [19–21], solute separation [22] and electronics applications [23].

The solute deposition at the contact line is a complex process [1,2,4,29-31]. Contact line pinning and contact angle hysteresis (CAH) play a critical role in formation of coffee-ring effect [59]. The evaporation rate and hence the capillary flow diverges at the contact line due to the relatively larger proportion of the liquid-air interface there [5,30]. For evaporating droplets of colloidal suspension, the particle deposition at the contact line can be ordered (square and hexagonal packings) or disordered depending on the magnitude of capillary flow [32]. Marin et al. observed that the capillary flow diverges towards the end of the evaporation process and hence a transition from ordered to disordered packing is observed [32]. The solute deposition process is also influenced by a number of other aspects such as the presence of electric double layer at the liquid-substrate interface [33], the thermal Marangoni flows [34], the ratio of the thermal conductivities of the substrate and liquid [35], surface charge of the substrate and particle surfaces [36], and even the shape of the particles [37,38]. Deposition of large particles are also influenced by the inward capillary push due to the decreasing height of the liquid wedge near the contact line [39]. Similar forces due to geometrical constraints in a different configuration formed unique packings of colloidal particles at the interface of liquid emulsion droplets in the presence of slow evaporation [40,41].

Several theoretical models were developed to predict the morphology of the deposit, the resulting film thickness and the solvent flux. The first reported models by Parisse et al. could estimate the film thickness upon complete evaporation [29,30]. Later, the works of Deegan et al. [4,31] and others [1,2,5,42-44] gave more complete mechanistic understanding of CRE. Theoretical models incorporating the factors such as the receding of the contact line [45,46], center-enhanced flux [47], presence of polymers [48–51] and surfactants [52] have shown to alter the morphology of the residues. Frastia et al. included the stick-slip motion of the receding contact line and observed the formation of multi-ring deposition of the solutes [53,54]. The multiphase model of Kaplan et al. showed that relative strength of the capillary flow and the evaporative flux influences the deposition pattern [55] as also demonstrated by Shen et al. [56].

1.1. Outline of this review

The physical insights obtained through theoretical and experimental investigations of CRE have not only been utilized to develop CRE-free manufacturing processes but also they inspired novel strategies exploiting CRE as a method for convective assembly. We review this multi-faceted phenomenon in two sections: (i) the strategies to suppress CRE and (ii) the approaches leveraging CRE to arrive at novel processes and materials. Within each section we classify the methods based on their working principle.

2. Suppression of CRE

CRE can be suppressed through one of the three physical strategies (i) preventing the pinning of the contact line; (ii) disturbing the capillary flow towards the contact line and (iii) preventing the particles being transported to the droplet edge by the capillary flows. We will first briefly introduce these three strategies then discuss them in detail in different sections.

The contact line pinning of a sessile droplet is characterized by the CAH [57–59]. The pinning force per unit length and the contact angle hysteresis are related as $f_p = \gamma\,(\cos\theta_a - \cos\theta_r)$ where γ is the surface tension and θ_a and θ_r are the advancing and receding contact angles, respectively. Minimizing the hysteresis will facilitate smooth receding of the contact line upon evaporation hence preventing the formation of ring-like deposits as also suggested by the theoretical models [45,46,53]. Experimentally, it can be achieved by evaporating droplets on low CAH superhydrophobic surfaces [64-68,70] or through CAH suppression via electrowetting [77].

When the evaporation-driven outward capillary flow is disturbed the solute transport to the contact line can be minimized or even totally avoided. This can be achieved by inducing additional flow fields inside the droplet, for example, by surface tension gradients (Marangoni flows) [5,12], electrowetting [13,77], electroosmosis [80] and acoustic streaming [84].

The transport of solute particles to the contact line can be prevented by utilizing the particle-particle interactions and/or the interaction of particles with the solid-liquid (SL) interface and liquid-gas (LG) interface [60,118]. In this strategy, solute particles can aggregate at the SL interface or form arrested structures at the LG interface altering the capillary flows. Other methods to prevent the transport of particles are acoustics and phase transition of the liquid during evaporation [8,9].

2.1. Preventing the contact line pinning using hydrophobic surfaces

Increasing the hydrophobicity of surfaces is often accompanied by decreasing CAH [59]. Lower CAH in essence means reduced contact line pinning which leads to suppression of CRE. It can be achieved by patterning of controllable surface wettability as reviewed previously by Tial et al. [62]. These methods include chemical modification [61,62] and physical modification [62-68,70].

The hydrophobization by chemical modification involves covering the surface with hydrophobic molecules such as self-assembled monolayers [61,62]. The physical modification involves patterning the surface to create microscopic roughness on it, for example, an array of pillars, which in turn decreases the effective contact area of the solid-liquid interface. When hydrophobized, such rough surfaces act as superhydrophobic surfaces. Two different types of droplet configurations are possible on such surfaces: Cassie or Wenzel states (Fig. 1a). In the Cassie state, a droplet sits on the pillars and its evaporation can produce ball-like spherical [67] or disc-like [68] deposit (Fig. 1b, c). In the Wenzel state, the liquid fills in between the pillars. Cassie to Wenzel transition of the droplet was studied previously [68,69]. It depends upon the balance between the Laplace pressure $P_L = 2\gamma/R$ and the capillary pressure $P_c = -4\gamma cos\theta_Y[\phi/(w(1-\phi))]$, where R is the radius of the droplet, θ_Y is the equilibrium contact angle, ϕ is the surface solid fraction and w is the pillar width. The capillary pressure decreases with increasing pillar pitch. As the droplet evaporates, the Laplace pressure increases due to the decreasing droplet radius. Cassie to Wenzel transition occurs when the droplet becomes small enough such that the Laplace pressure exceeds the capillary pressure. It means that there

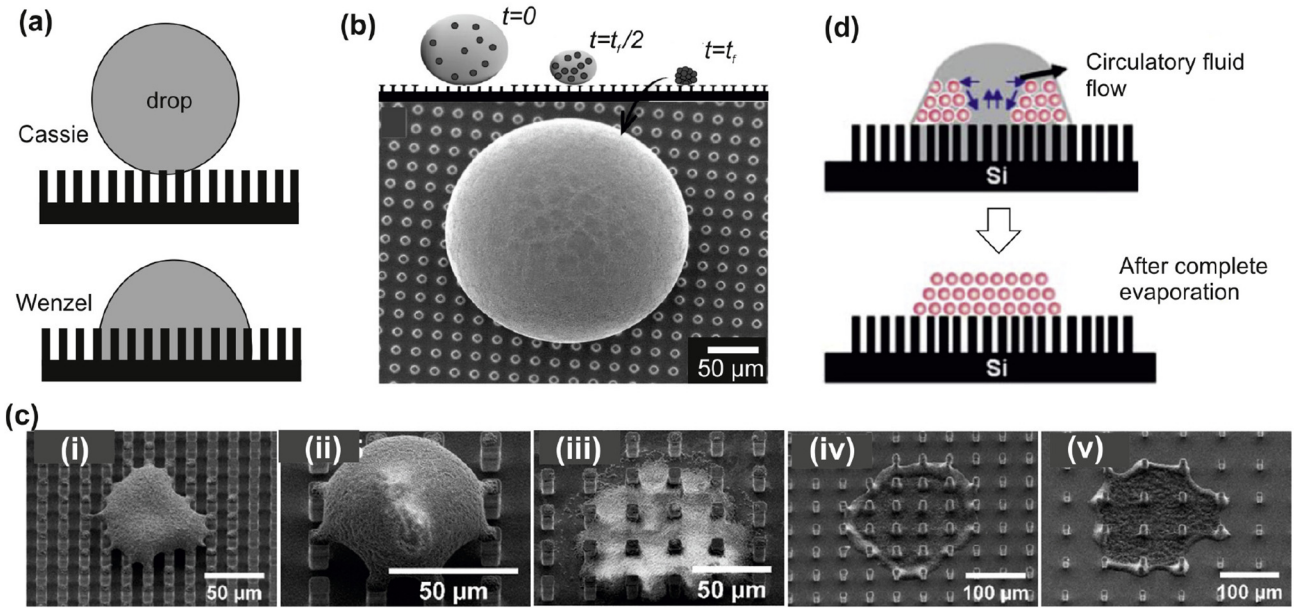

Fig. 1. The CRE on superhydrophobic surfaces. (a) A droplet can stay on top of the micropillars (Cassie state) or fill in between the pillars (Wenzel state). (b) Evaporation of a colloidal droplet on superhydrophobic surface produced a spherical particle conglomerate. Adapted with permission from: [67] Copyright ©2012, National Academy of Sciences, USA. (c) SEM images of representative particulate deposits on the five different surfaces show the influence of surface morphology on deposit pattern. Surfaces (i) and (ii) show Cassie deposits whereas (iii) to (v) show Wenzel deposits. Adapted with permission from: [68] Copyright ©2014, American Physical Society. (d) Drying in the Wenzel configuration also can result uniform deposition. Adapted with permission from: [70] Copyright ©2012, Royal Society of Chemistry.

exists a critical pitch above which Wenzel deposits are formed [68]. Wenzel state is often associated with pinning. However, when nanotextures are applied on superhydrophobic surfaces, droplets in the Wenzel state can also have slipping contact lines [71]. Gelation of the particles at the edge of a Wenzel droplet can result in an inward circulatory flow of liquid suppressing CRE [70] (Fig. 1d). It is also demonstrated that on surfaces with small CAH the solutes with low surface activity (say copper sulfate) formed spot-like residues [74].

The suppression of CRE using (super)-hydrophobic surfaces is simple as they do not require any external involvement during the drying of droplets. However, the preparation of superhydrophobic surfaces is expensive. Another issue is the strong pinning of the contact line when surface active/adsorbing molecules are present in the droplet as in the case with biological fluids such as blood and urine. Biological sample have variety of molecules that adsorb readily on the surfaces through hydrophobic or non-specific interactions. Thus, suppression of CRE in biological fluids using of hydrophobic surfaces is still an open challenge. In such scenarios, strong convective flows can be introduced in the droplet to minimize the adsorption induced CAH as a potential solution.

2.2. Electrowetting

On hydrophobic and partially hydrophobic surfaces, pinning can occur when the CAH or solute concentration is high. If CAH is high, during when the contact angle decreases to the receding angle, typically a few seconds depending upon the rate of evaporation, solutes can accumulate at the contact line. Such accumulation produces ring-like deposits only if the duration of pinning is above a critical value for a given substrate-solute system [72]. On the other hand, short pinning time even with high initial solute concentration can minimize CRE producing smaller inner rings [73]. The pinning induced by deposition becomes more prominent when the solute is nanoparticles as they can flow into the microscopic regions of the droplet edge.

In the presence of solute particles in the droplet, electrowetting (EW) can ensure efficient slippage of the contact line on (partially)-hydrophobic surfaces [75,76]. In EW configuration, a droplet is deposited on a dielectric layer of thickness d and dielectric constant ϵ_d covering an electrode (Fig. 2). When a voltage U is applied between the droplet and the electrode an electric force per unit length $f_{el} = \epsilon_d \epsilon_0 U^2/2d$ (ϵ_0: vacuum permittivity) pulls the contact line outward, overcoming the pinning forces. In AC (alternate current) electrowetting (ACEW), the contact line moves periodically, thereby de-pinning it continuously from the pinning sites. It allows the contact line to recede freely as the droplet evaporates [76]. Additionally, ACEW generates circulating flow inside the droplet, which mixes the solutes continuously. Flow is generated at higher frequencies of the applied voltage, typically a few kHz. The slipping contact line and the internal flow produce concentrated spot-like residues [13,14,77] (Fig. 2). Such concentrated residue of analytes increased the signal strength in MALDI spectrometry [13,14].

Theoretical studies have demonstrated that drying a droplet in an electric field in other configurations also suppresses CRE [78,79]. For example, the application of a Gaussian potential near the edge of a droplet deforms its interface due to the Maxwell stress. The deformation is in such a way that it drives the bulk of the droplet towards its center eventually resulting in the suppression of CRE [78]. Zhang et al. studied the effect of electric field on evaporating nanodroplets of salt-water using molecular dynamics simulation [79]. They applied DC (direct current) electric fields along uni-axis, and AC electric fields axisymmetric, both parallel to the substrate. The application of electric fields parallel to the substrate is equivalent to the EW configuration with interdigitated electrodes [77]. With DC fields above 0.03 V/Å, the salt crystals formed a ribbon-like pattern along the direction of the field. Low frequency AC electric fields stronger than approximately 0.006 V/Å gave spot-like residues. At higher frequencies i.e. typically a few tens of GHz, ring-like patterns reappeared because the time scale of the periodically varying electrophoretic force became comparable to the local equilibration time scale, thus nullifying the effect of the electric field.

Molecular adsorption on hydrophobic surfaces can decrease the efficiency ACEW induced CRE suppression. The gradual accumulation of adsorbing molecules at the contact line prevents its oscillations. However, the internal flow inside the droplet minimizes adsorption. The working principle in ACEW is purely hydrodynamic implying that the suppression is achieved by the contact line oscillations and the internal flow [13,14,77]. No electric field exist inside the droplet if the liquid is conducting. It should be noted that EW under DC fields cannot generate contact line oscillations. The inconvenience with the configuration having a wire inserted into the droplet can be avoided by using EW substrates with interdigitated electrodes [77]. In short, EW offers a feasible solution to suppress CRE even in the presence of high concentrations of solutes in the droplet when the substrate surface is (partially)-hydrophobic.

2.3. Electroosmotic flow

The capillary flow acting on the electric double layer at the solid-liquid interface generates streaming potentials and influences the solute transport [33]. The existence of the electric double layer can be exploited to generate electroosmotic flow (EOF) by externally applied electric fields inside the droplet [80]. This is achieved by placing a circular electrode around the rim of the droplet and a point electrode at the center (Fig. 3). The electric field applied between the point electrode and the circular electrode generates a radial EOF near the substrate. EOF velocity is given by $v_{eof} = -\epsilon_0\epsilon_r\zeta E/\eta$ where, E is the electric field, ζ is the zeta potential of the substrate and ϵ_r is the dielectric constant of the liquid. When the radially inward EOF overcomes the outward capillary flow, CRE does not occur. This method requires precise deposition of the droplet on the electrodes and may also involve minor heating effects. However, it is non-invasive as it avoids the addition of surface active materials.

2.4. Vibrations and acoustics

Substrate vibrations have shown to produce uniform layers in the convective depositions of colloidal monolayers [81] and in spray coating for organic solar-cell applications [82]. The acceleration of the surface deforms the air-liquid interface and the resulting pressure variations induce local flow of the liquid. This flow near the substrate prevents the clustering of the particles at the contact line and results in uniform depositions.

Recently, surface acoustic waves (SAW) [83] were used for altering the evaporative patterns [84–86]. Mampallil et al. demonstrated that CRE can be suppressed when the droplet is dried on a surface where SAW propagates (see Fig. 4a). The SAW creates standing pressure waves in the droplet. The acoustic force pushes the particles towards the nodes of the standing waves. This force (say, along x direction) is given as $F_{ac} = 4\pi a^3 k E_{ac}\Phi\sin(2kx)$, where a is the diameter of the particle, k is the wave number, E_{ac} is the time-averaged acoustic energy density, and Φ is the acoustic contrast factor that depends on the density and compressibility of the particle and the liquid. When the acoustic force is higher than the drag force due to the capillary flow, the particles are trapped in the pressure nodes in the bulk of the droplet (Fig. 4b). Trapping of particles in pressure nodes prevents the transport of the particles to the contact line (Fig. 4c, d). Mhatre et al. studied the particle deposition on SAW propagating surfaces both theoretically and experimentally [85]. They derived governing conditions for the formation of stripes to films and verified the conditions experimentally.

The method based on acoustics has the advantage that it is independent of the particle shape, density, nature of the liquid and the wettability of the surface. The method is also suitable with biological samples [84]. The substrate placed on the acoustic transducer should be of an elastic material such as glass, silicon or metals. The surface requires no physio-chemical modifications. This method is not effective when the particle size is small such that the acoustic force becomes smaller than the drag force. For particles of diameter typically above 100 nm, this issue can be overcome by increasing the frequency and/or the acoustic energy, without causing excessive heating of the droplet. When acoustic trapping is not effective, acoustic streaming flow can be used, which produces concentrated residue even with nanoparticles [86].

2.5. Marangoni flow

Due to the endothermic nature of evaporation, the liquid-gas interface of the droplet is cooler than the bulk liquid. Any small perturbation in the surface temperature creates surface tension gradients resulting in the Marangoni flow [87–89].

Influence of Marangoni flow on solute deposition has been studied theoretically and experimentally [35,52,87]. For an evaporating sessile droplet the direction of Marangoni flow depends on the relative thermal conductivities of the liquid and the substrate. When the ratio of substrate and liquid thermal conductivities (k_R) is below 1.45,

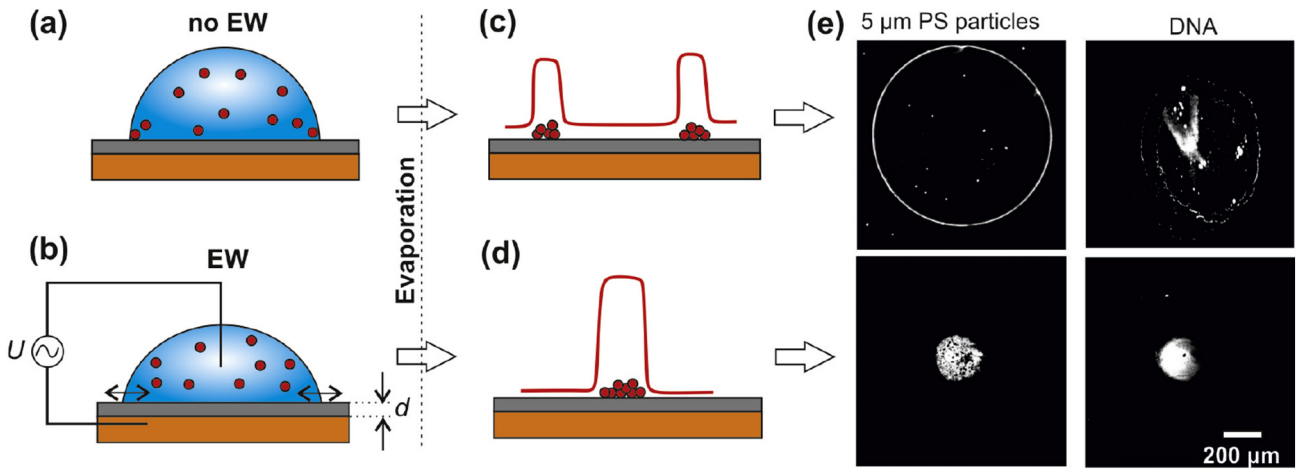

Fig. 2. Electrowetting and CRE. (a) Undisturbed evaporation and (b) evaporation under ACEW (150 V and 6 Hz). (c, d) Cartoon of the surface profile after evaporation in the both cases. (e) The residues with PS particles and DNA (refs. [13,77]).

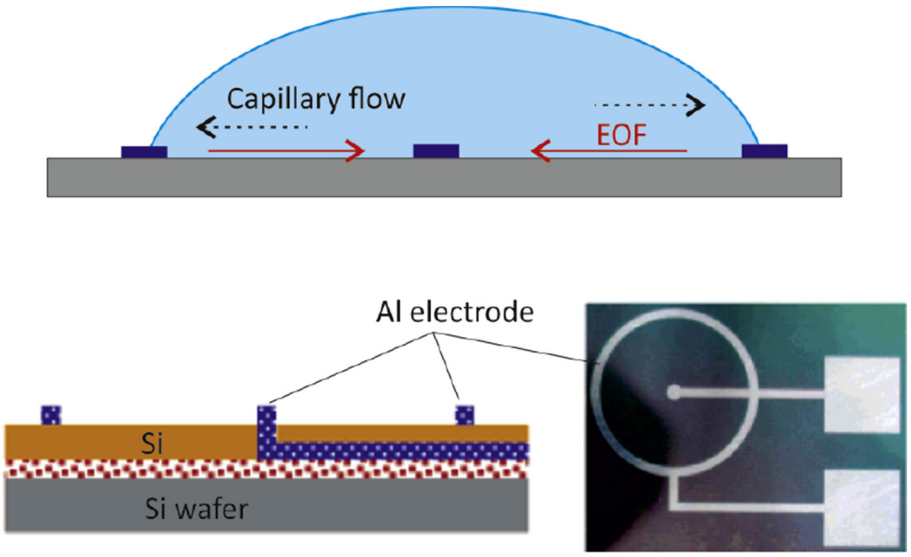

Fig. 3. EOF based suppression of CRE. Using surface patterned electrodes electric field is applied in the droplet. The EOF near the surface can oppose the capillary flow (dashed arrow). The schematic of the cross-section and top view of the electrodes are also shown.
Source: Copyright ©2006, American Chemical Society.

the edge of the droplet is the coldest and the direction of the thermal Marangoni flow along the substrate is inward towards the center of the droplet [35] (Fig. 5a).

When the direction of the Marangoni flow is radially inward and its characteristic velocity $v_{Ma} \sim \frac{\partial\gamma}{\partial T}\frac{\Delta T}{\eta}$ is bigger than the outward capillary flow, particles are concentrated at the center of the droplet. In the case of water droplets, the thermal Marangoni flow is weak [1,2,90]. However, it is considerable in volatile non-aqueous based liquids [91]. The thermal Marangoni flow can be enhanced by elevating the temperature of the substrate [92,93] resulting in an increased solute concentration near the center of the droplet [92]. An increased temperature also increases the outwards capillary flow producing a ring as well. The result is a spot-inside-ring or an eye-like pattern. The effect of buoyant motion of the liquid from

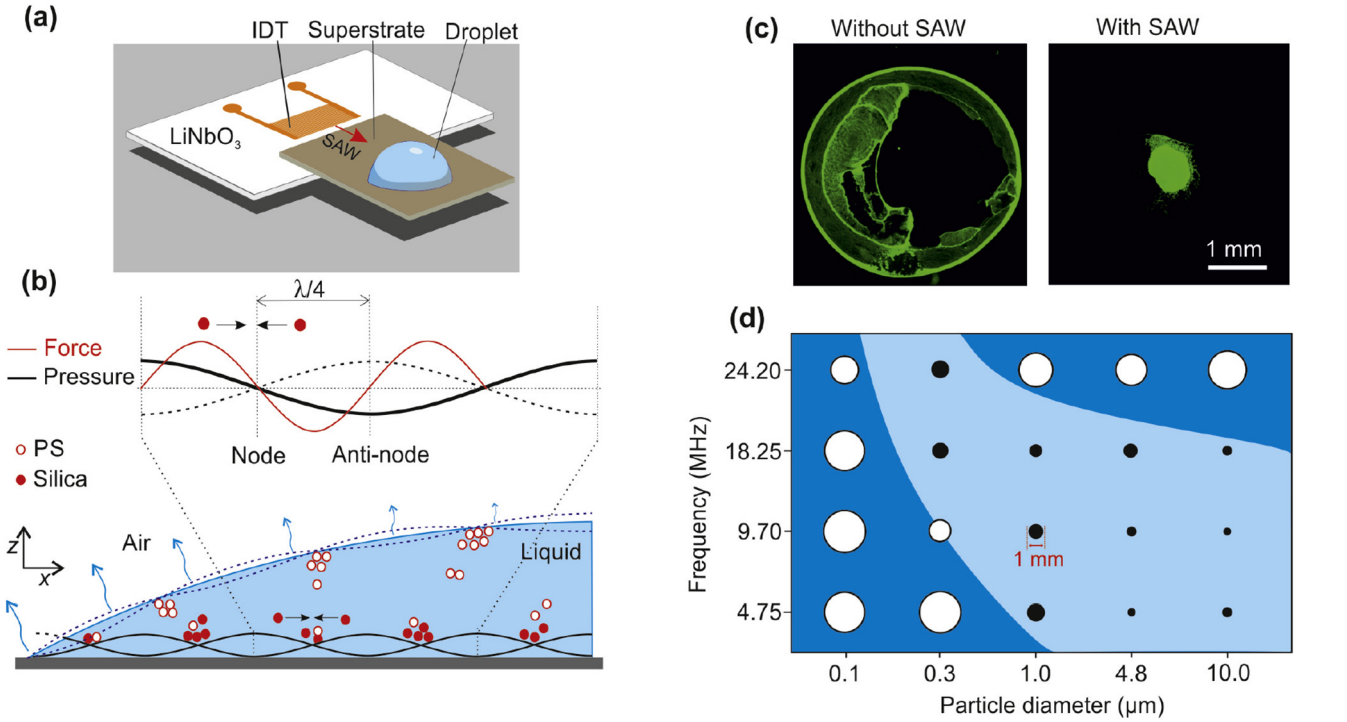

Fig. 4. Acoustics and CRE. (a) A droplet is placed on a 'superstrate', coupled to a piezoelectric device (IDT) that generates surface acoustic waves (SAW). (b) The particles do not reach to the contact line as they are trapped in the nodes of the standing capillary waves and pressure waves. Heavier silica particles get trapped in the pressure nodes near the superstrate surface. (c) Evaporation of a droplet with dispersed PS particles of diameter 1 μm under SAW (frequency 10 MHz; power 30 dBm) produced spot-like residue. (d) The range of frequencies and particle sizes at which a successful suppression is obtained. The filled circles indicate a successful suppression. At higher frequencies larger particles obstructed the receding contact line and produced coffee-rings (Ref. [84]).

the hot substrate to relatively cooler liquid-air interface is often negligible [92].

The droplet surface can be locally heated using a laser beam to generate radially inward flow [94]. In this study, an infra-red laser of wavelength 2.9 μ m (as water has strong absorption at this range) was irradiated at the liquid-air interface of the droplet (Fig. 5b). When the laser exposure time was at least 60% of the total evaporation time of the droplet CRE was fully suppressed. The residue morphology can be varied from uniform disc to spot-like deposition either by increasing the exposure time or decreasing the ratio between the laser spot size and the droplet diameter (Fig. 5c, d) [94].

Without rising the temperature of the system strong Marangoni flow can be generated mixing solvents [6,23,95,96,99] or adding surfactants [1,2,18,90,100,101] in the liquid. Surfactants decrease the surface tension of the liquid (say, water). As the liquid evaporates the concentration of the surfactants increases locally, generating strong gradients in the surface tension. The resulting Marangoni flow can overcome the capillary flow. Sodium dodecyl sulfate is an example of a commonly used surfactant. In bacterial systems, biologically produced surfactants can also induce Marangoni flow and suppress CRE [102]. Marin et al. showed that the nature of surfactant (ionic or non-ionic) is important in determining the residue shape. Their particle tracking measurements showed that the convective flow can reverse direction depending upon the nature of the surfactant by making the liquid-air interface either rigid or elastic [103].

Michen et al. demonstrated that addition of bovine serum albumin (BSA) to suspensions of nanoparticles avoided drying artefacts in the sample preparation for transmission electron microscopy [104]. In this process, BSA not only stabilized the individual particles against aggregation but also induced Marangoni flow and improved wetting on the solid surface. The optimum concentration of BSA was estimated depending upon the volume fraction of particle in the suspension and also the particle properties. Similarly, addition of low amount of ethylene glycol (10–30 vol%) in colloidal suspensions produced uniform deposits [96,97].

Marangoni flow is very strong in the drops of binary mixtures, for example, water and ethanol mixture. Here, one liquid being more volatile than the other, different flow regimes exist during the evaporation. As shown by Zhong et al., water-ethanol binary mixture drop suspended with alumina nanoparticles demonstrates three distinct regimes: the initial strong flow that takes the particle to the liquid-air interface; Marangoni flow; and evaporation of the water content [98].

Certain applications, for example, biochemical analyses do not favor CRE suppression methodologies using additives such as surfactants [1,2,18,90,100,101] and proteins [104]. Majumder et al. demonstrated a method that avoids additives by simply drying an aqueous droplet in an atmosphere containing ethanol vapor [105]. The preferential evaporation of the water at the contact line generates gradients in the surface tension, which drive strong recirculating Marangoni flow. This method was used for depositing catalyst nanoparticles homogeneously for the purpose of growing single-walled carbon nanotubes as well as manufacturing plasmonic films of gold nanoparticles [105].

Marangoni flow based methods require either heating of the liquid or addition of surfactants. Thus, it may not be suitable for applications in which heating or chemical alteration of the sample is undesirable. On the other hand, chemical additive induced Marangoni flow offers an easy solution to overcome the CRE. It does not require any physical interference during the evaporation and is independent of the system parameters. This method is thus suitable in most of the printing applications. However, sample preparation processes for biochemical analyses may not prefer such chemical addition based methods. In Marangoni flow based methods, dynamic control of the suppression process, for example, as in the case of EW, EOF or acoustics, is not possible.

2.6. Interactions at solid-liquid and liquid-gas interfaces

Various investigations have shown that tuning the particle-particle interactions [106] and particle-interface interactions [107,108] can lead to the suppression of CRE. The particle-particle

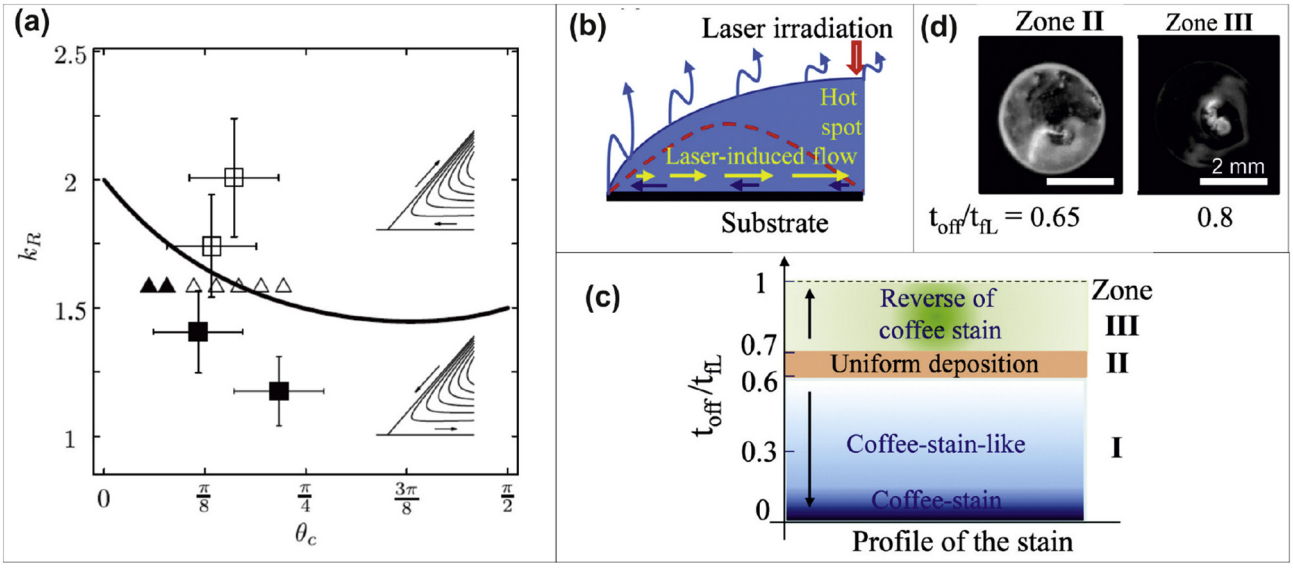

Fig. 5. Marangoni flow and CRE. (a) Experimental observations (squares) and numerical calculations (triangles) of the circulation reversal in evaporating droplets. From top to bottom, the squares represent evaporation of chloroform, isopropanol, ethanol and methanol on polydimethylsiloxane surface. The open symbols represent that the observed direction of circulation is consistent with temperature decreasing with distance from the contact line and the closed symbols represent the reverse circulation. Adapted with permission from: [35] Copyright ©2007, American Physical Society. (b) Particle deposition can be controlled by heating the surface of a colloidal droplet using a laser beam. The laser beam induced flow (yellow arrows) is in the opposite direction to the capillary flow (black arrows). The red dashed line indicates the droplet profile towards the end of the evaporation. (c) The shape of the stain depended on the ratio of exposure time (t_{off}) and the evaporation time (t_{fL}). (d) Optical images of residues (0.5 μm PS particles) depending upon the ratio t_{off}/t_{fL}. Adapted with permission from: [94] Copyright ©2016, Royal Society of Chemistry.

interactions can prevent their transport to the contact line as the particle aggregates settle down on to the substrate surface. The aggregation can be achieved for example, by increasing the salt concentration of the liquid or tuning the pH of the liquid to reduce the inter-particle electrostatic repulsion [109]. When aggregation is present, the shape of the residue depends upon the evaporation rate [110,111]. Dugyala et al. showed that when the evaporation rate was lowered uniform disc-like deposits were formed [111]. Other examples for particle-particle interaction preventing CRE are the formation of transparent films of TiO_2 nanoparticles [112], uniform films by silver nano-ellipsoids [113] and uniform films when casting a colloidal suspension of graphene oxide and titania on glass surface [114]. Such uniform hybrid films can have applications in the deposition of high-quality membranes from liquid phases [114].

The interactions of particles at the solid-liquid (SL) interface, for example by DLVO (Derjaguin Landau Verwey Overbeek) interactions (i.e. the sum of electrostatic and van der Waals forces), can mitigate the transport of particles to the contact line and produce homogeneous residues [36,109]. The surface charge of the particle and the substrate can be controlled by changing the pH of the liquid [36] or adding surfactants into the liquid [115]. The surfactants adsorb on the surface of the particles and substrate. Therefore, the charge of the surfactant molecules can be utilized to alter the particles and the substrate interactions. [115]. Bhardwaj et al. showed that competence of three convective mechanisms i.e. the capillary flow, particle migration to the solid surface by DLVO attractive forces and the Marangoni flow determines the morphology of the residue [36] (Fig. 6a). Using ellipsoidal particles of different aspect ratios Dugyala et al. showed that CRE was stronger when the strength of particle-particle repulsion was higher than the particle-substrate attraction. However, CRE was suppressed when both particle-substrate and particle-particle interactions were attractive [109] (Fig. 6b).

When particles adsorb to the liquid-gas (LG) interface they deform the meniscus generating particle-particle attractive forces of capillary nature [116,117] (Fig. 6c, d). This interaction is strong and long-range particularly between ellipsoidal particles, which eventually generates homogeneous residues (Fig. 6e) [118]. This method works even with mixtures of spherical and ellipsoidal particles provided that the sphere diameter is larger than the minor axis of the ellipsoid. Even a small amount of ellipsoidal particles, i.e. about 130 times lesser volume fraction compared to the spherical ones, could suppress CRE [118].

The trapping of particles at the LG interface depends on the curvature of the interface [119] and wetting of the particle surface. It is not possible to trap a particle when its surface is very hydrophilic. This issue can be overcome by introducing surfactants in the liquid. In this case, the interactions depends on the charge of both the particles and the surfactant molecules [120,121]. When oppositely charged particle-surfactant mixtures were used, the adsorption of the surfactants onto the particle surface enhanced the affinity of those particles to the LG interface. This affinity was stronger at intermediate concentrations of the surfactant as the particles became more hydrophobic (Fig. 6f, g). The energy required to bring a particle from the interface to the water phase is given by $E_{iw} = \frac{\pi}{4}a^2\gamma(1-\cos\theta)^2$, where a is the diameter of the particle. As a result, an increase in the particle hydrophobicity i.e. an increase in θ should cost more energy to bring the particles back into the water. Therefore, increasing the hydrophobicity tends the particles to remain trapped at the interface. In the converse case, when like-charged particle-surfactant mixtures were used, particles did not adsorb to the LG interface and CRE was observed [121].

The particle affinity to the LG interface can be controlled by modulating the surfactant-particle interactions optically [125]. Photosensitive cationic surfactant AzoTAB changes between *trans* (less hydrophilic) and *cis* (more hydrophilic) states when irradiated with blue light. The trans-molecules easily adsorbed on to the anionic polystyrene nanoparticles. This allowed tuning the particle interaction with LG interface optically, achieving controllability on the shape of the dried patterns [125].

Evaporation of aqueous suspensions of poly(N-isopropylacrylamide)(pNIPAm) microgel (hydrogel) particles produces uniform deposition [122,123]. Microgel particles are spherical polymeric networks swollen when dispersed in a solvent. pNIPAm is thermally sensitive, which shows a volume phase transition around 31 °C in aqueous media. The pNIPAm microgel particles adsorb at the LG interface during the evaporation [124] preventing their non-uniform transport to the contact line during the evaporation [122,123].

The particles suspended in the liquid can be captured at the LG interface by allowing it to descent rapidly by fast evaporation [126,127]. The average descending rate of the interface is h/t_f, where h is the initial droplet height and t_f is the evaporation time. The particles diffusing vertically upwards are captured when the descending rate of the interface is faster than the average diffusion rate, $2(Dt/\pi)^{1/2}$ (D: the diffusion coefficient), of the particle. Once the particles are trapped at the LG interface, the resulting deposit becomes homogeneous (Fig. 7).

The methods utilizing the interfacial interactions are easy to be deployed as they do not require any external devices to generate forces (such as hydrodynamic, electric and acoustic) that interfere with the capillary flow during the evaporation. This feature makes the technique widely applicable on a range of substrates and in applications like inkjet printing. Tuning the liquid properties (say, pH) or addition of surfactants forms uniform deposition of colloids in the droplet. Particularly, the method using ellipsoidal particles does not require any such tuning of the chemical environment of the liquid and thus it is suitable when chemical additives are not desired. Even a small amount of ellipsoidal particles can change the deposition pattern of a droplet containing majority of spherical particles. The residue formation with particle-particle interaction can be further investigated with mixture of particles having different properties (size and surface species). It may generate new patterns as the mutual interactions between the particles vary.

2.7. Transition of liquid property

Modifying the liquid properties is a common strategy adapted for avoiding CRE in inkjet printing [8,9]. Uniform deposits can obtained by altering the composition of the colloidal ink solution to avail of the Marangoni effects and to induce fast drying [6,7,130-133].

One may assume that simply increasing the viscosity of the liquid can suppress the capillary flow. It is possible only if the viscous effects dominate the capillary effects. The relative importance of both these properties can be compared by the capillary number, $Ca = \eta v_{rad}/\gamma$. Putting typical numbers for the capillary flow velocity $v_{rad} = 10$ μm/s, for water we obtain $Ca \sim 10^{-7}$. It implies that for viscous effects to play a major role, i.e. for $Ca \geq 1$, there should be at least 10^7 fold increase in the viscosity [128]. Therefore, in practice increasing the viscosity is not a recipe for suppressing the capillary flow.

Since very high viscosity is a bottleneck in printing applications, viscous liquids with tailored rheological properties are needed. For example, liquids that can undergo sol-gel transition i.e. change from a easily flowing low viscosity solution into a complex fluid that flows above a given shear. Droplets of colloidal suspensions containing laponite, a synthetic clay that swells to form a gel when dispersed in water, does not produce CRE due to the sol-gel transition of laponite during evaporation [128,129]. As the droplet evaporates, the laponite concentration increases forming a gel. It resists the capillary stresses and the resulting flow of the particles. The advantage of sol-gel transition is more than simply increasing the viscosity with additives as the resulting gel is a yield stress fluid. For example, laponite

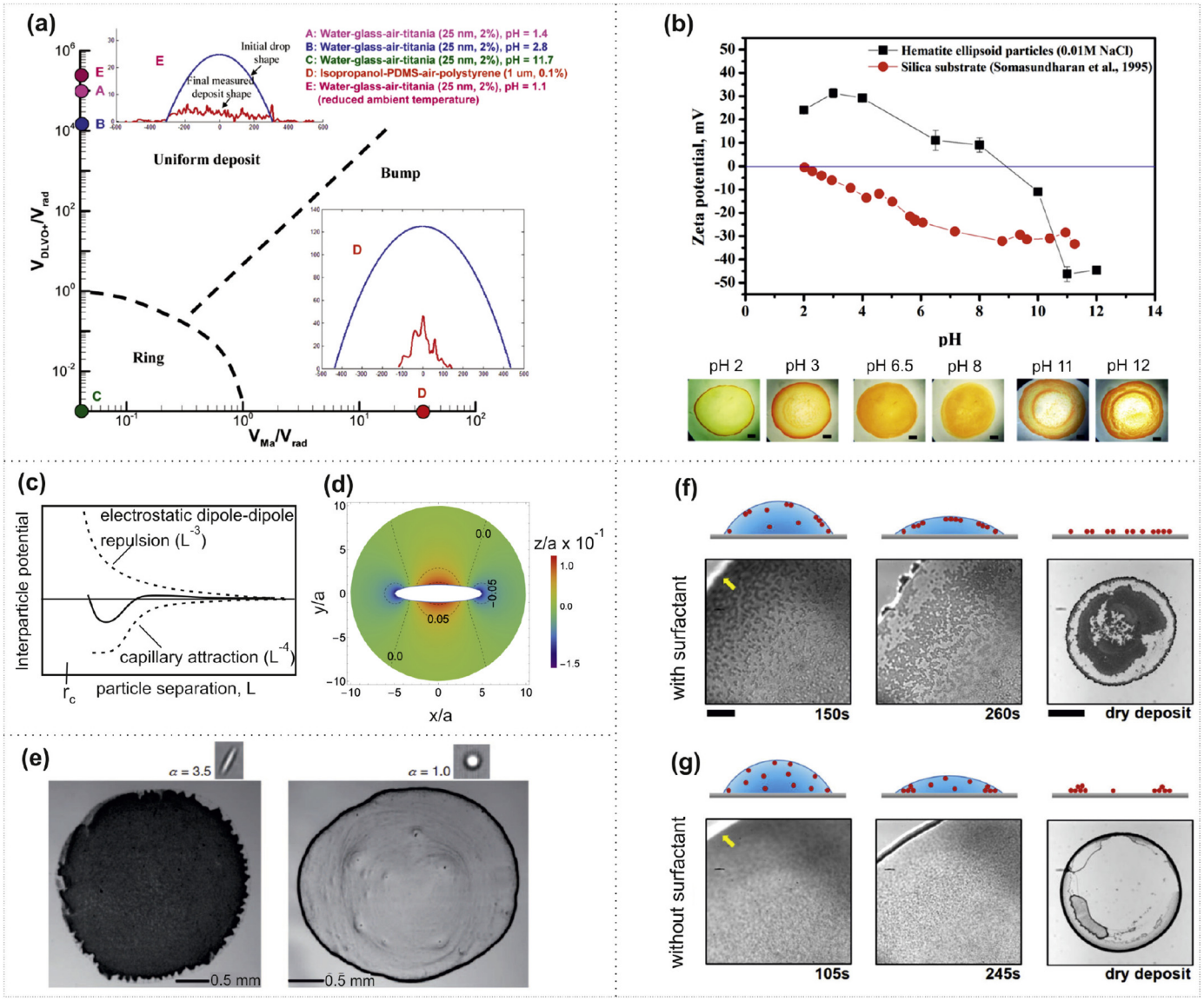

Fig. 6. Interfacial effects and CRE. (a) Phase diagram for evaporative self-assembly of nanoparticles. The final pattern shape is determined by the relative strength of three characteristic velocities: capillary flow (V_{rad}), velocity due to attractive DLVO forces (V_{DLVO+}), and Marangoni flow (V_{Ma}). Adapted with permission from: [36] Copyright ©2010, American Chemical Society. (b) Optical images of dried patterns obtained with hematite ellipsoidal particles on a glass slide at different pH values. The zeta potentials of the particles and the glass surface are also shown. Intermediate pH values generated uniform deposits. Adapted with permission from: [109] Copyright ©2015, American Chemical Society. (c) The sketch of overall potential in the interaction of two particles at the LG interface. At small distances the capillary attraction, which scales as L^{-4}, is strong enough to overcome the electrostatic dipole-dipole repulsion, which scales as L^{-3}. r_c is the minimum distance between the particles. Recreated from (recreated from [116]).(d) Deformation profiles of the LG interface around an ellipsoidal particle with aspect ratio 5.0. Adapted with permission from: [117] Copyright ©2014, American Chemical Society. (e) Uniform deposition occurred when colloidal droplet containing ellipsoidal particles dried on solid surface. α is the major-minor axis aspect ratio of the particles. Adapted with permission from: [118] Copyright ©2011, Nature. Evaporation of a droplet containing anionic PS particles (0.5 μm diameter) with (f) and without (g) surfactant (DTAB). For the droplet containing DTAB, particles accumulated at the interface eventually leading to a fairly homogeneous pattern. For the surfactant-free droplet, particle adsorption at the LG interface was much weaker, thus showing CRE. Adapted with permission from: [121] Copyright ©2015, American Chemical Society.

suspensions are highly viscous, yet above a given shear rate they flow like a low viscosity liquid.

Eales et al. studied the evaporation of polymer droplets numerically to understand the ways to control the residue formation [50,51]. They found that polymers with larger molecular weight mitigated CRE. Similarly, a reduction in the Péclet number, which implies a diffusion dominated transport, also mitigated CRE. This is because the diffusion of the polymer counteracts its transport by the weak capillary flow. Experimental studies also show that the dried pattern depends on the molecular size. With high molecular weight the contact line moves slowly leaving a continuous layer of polymer [134].

Droplets containing pNIPAm-modified colloids formed homogeneous residues due to faster monomer polymerization during evaporation [135]. Van den Berg et al. achieved thermally induced gelation of TiO_2 ink containing special polymers [136]. Here, the colloidal stability was initially achieved by the adsorption of polymers (poly(vinyl methyl ether) block-poly(vinyloxy-4-butyric acid)) on the surfaces of the particles inducing steric repulsion. When the temperature was raised above 33 °C, poly(vinyl methyl ether) became

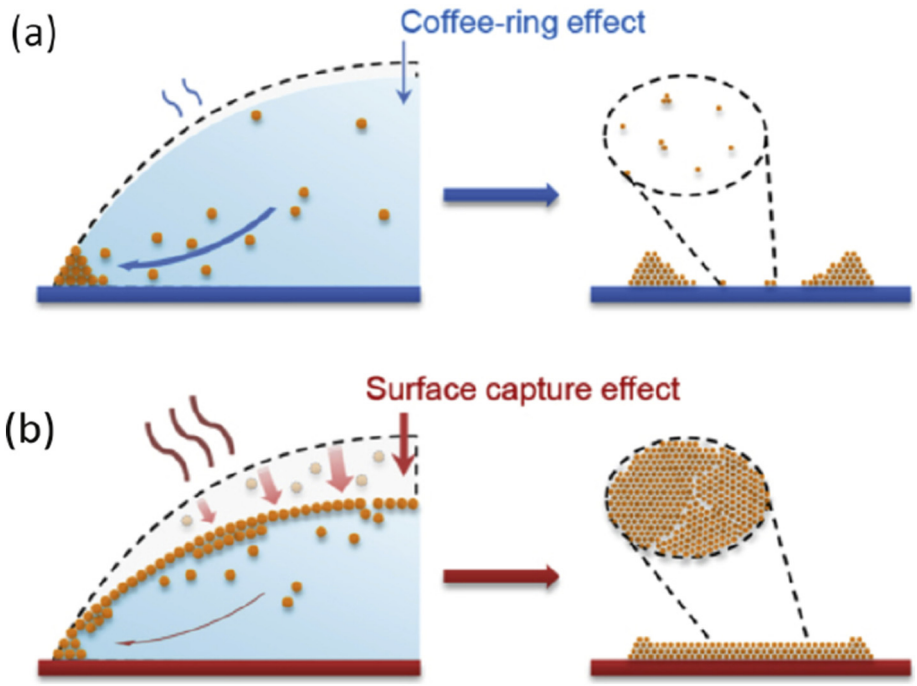

Fig. 7. Thermally induced surface capturing. When temperature is raised the interface descends more quickly than particle diffusion, capturing the particles at the interface. It produces uniform deposition (see ref. [127]).

insoluble and the adsorbed layer of polymers collapsed on the surface of the particle destroying the colloidal stability. The resulting aggregation and increase in viscosity eliminated CRE.

The substrate temperature can also be a control parameter in gelation as demonstrated by Soltman et al. [137]. They inkjet printed uniform lines without CRE by optimizing the substrate temperature, deposition frequency and the droplet spacing using the polymer, poly(3,4-ethylenedioxythiophene)poly(styrenesulfonate) on glass surfaces coated with poly(4-vinylphenol) dielectric. Higher temperatures (above about 30 °C) of the substrate produced CRE but lower temperatures suppressed it [137].

Evaporation of water droplets containing lysozyme was studied using AFM and optical microscopy [138]. Lysozyme is a globular protein, for example, present in human tears and saliva. As the droplet diameter varied from 1 to 50 μ m, above a critical diameter the shape of the residue changed from cap to ring. This critical diameter of the droplet systematically increased with lysozyme concentration. Below the critical diameter the Péclet numbers (*Pe*) were small. When $Pe < 1$, the lysozyme particles were transported mainly by diffusion and the deposit patterns were strongly depended on the concentration. It means that before considerable amount of particles reached at the droplet-edge gelation occurred there due to evaporation.

2.8. Humidity cycling

It was shown that modifying the local atmospheric conditions, for example, switching between evaporation and condensation processes suppresses CRE of polymer droplets [141]. When the residue was exposed to the solvent vapor for an optimum duration and dried again, its morphology changed from ring to disc. The numerical studies by Eales show that CRE is eliminated due to the refluidization of gelled regions during the condensation [142]. Refluidization brings back the spherical cap shape to minimize the surface energy. The process of regaining the spherical cap shape induces an inward flow towards the center of the droplet. The restoring time of the spherical cap shape during the condensation phase sets an optimum duration of the condensation and evaporation phases. The advantage of the humidity cycling method is that it does not require tuning material properties or introduction of any external fields. This method is suitable for solutions that can dry and refluidize for example, polymer solutions.

2.9. Porous substrates

When droplet evaporation occurs on porous substrates the residue morphology depends upon factors such as porosity and the depth of the pores [139]. When the solvent is fully imbibed into the pores the competition between the rate of particle motion to the contact line and the rate of solvent infiltration determines the final deposition pattern. The CRE is suppressed when the infiltration into the pores is faster. If the infiltration of the solvent is not complete, then the competition between particle motion and evaporation rate of the remaining liquid governs the final deposition patterns. Similar conditions govern the evaporation and pattern formation on paper substrates [140].

2.10. Other methods

Other methods found in the literature are depositing multi droplets and using inclined surfaces. Depositing multiple droplets subsequently on an initially formed non-uniform residue can eventually form a deposit without thick edges [143]. The principle of this technique lies in the competition between the time scales of particle diffusion and solvent evaporation from the printed deposit. The residue formation on inclined surfaces [144] is also interesting in view of the suppression of CRE. Simply tilting the substrate at an angle of 10° and raising its temperature (50 °C) formed a uniform film of silver nanoparticles and nanowires, which was used for SERS studies [16,145].

2.11. Advantages and limitations

Fig. 8 provides a compact overview of the methods utilized to suppress CRE. The rows are arranged to identify the methods in columns based on their mode of action, advantages and limitations. The first three rows point out which one of the three physical approaches the methods utilize, namely de-pinning, disturbing the capillary flow and trapping the solute. The advantages and limitations are categorized from an application point of view.

As shown in Fig. 8, every method has its own successful working range and limitations. A common scenario where most of the methods are pushed to the limits is the presence of nanoparticles in the liquid. The nanoparticles quickly move into the microscopic regions of the liquid wedge at the contact line inducing strong pinning. However, such pinning is minimized on highly hydrophobic surfaces and when externally induced flow (e.g. by Marangoni effect, ACEW and SAW) is much stronger than the capillary flow. The hydrophobic surfaces enhance adsorption of hydrophobic molecules (say, in biological samples). The hydrophilic surfaces minimize such adsorption but they in general increase the CRE because of the strong capillary flows due to the small contact angle. Therefore, methods having the combination of the use of moderately hydrophilic surfaces and externally induced strong flow will be an optimum solution to prevent CRE.

When external forcing is applied during evaporation as in ACEW and SAW, the accompanying devices make the method unsuitable for integration with conventional systems (say, printers). This limitation may not exist in the case of solute or solvent modification. The shape of the suppressed residue is also important depending upon the application. In the case of printing disc-like uniformly distributed residue is preferred. Such deposition is also useful in the sample preparation for SERS measurements. In the sample preparation for MALDI concentrated spot-like residues are preferred. Spot-like residues are formed when the contact line is continuously de-pinning during the evaporation. However, a disc-like, large and uniform residue requires the contact line to be pinned but the solutes are not transported to there. This scenario can be achieved in methods that trap the solute, namely, the ones using acoustic trapping at high frequencies and interactions at LG and SL interfaces. Dynamic controllability in the suppression methods helps to control the shape of the residue. It also helps in patterning particles with various designs broadening the applications.

3. Utilization of CRE

Evaporation of droplets can be exploited as a method to concentrate its solutes in it. Evaporation of the solvent can increase the analyte concentration making the reactions more probable [146,147]. When strong CRE exists, the solute is deposited at the contact line increasing their concentration there. This deposition of solutes and particles are exploited as a pre-concentration method

		Hydrophobic surface	Electrowetting	Electroosmotic flow	Acoustics	Marangoni flow (thermal)	Marangoni flow (surfactant)	Particle- **LG** interface interactions	Particle- **SL** interface interactions	Transition of liquid property	Humidity cycling	Porous substrates
Mode of action	De-pinning contact line	✓	✓									
	Disturbing capillary flow		✓	✓	✓	✓	✓				✓	✓
	Trapping solute				✓			✓	✓	✓		
Advantages	Dynamic control		✓	✓	✓							
	Compatible with wide substrate-wettability			✓	✓	✓	✓	✓	✓	✓	✓	
	Compatible with particle denser than liquid				✓				✓			
	Compatible with biological samples			✓	✓	✓	✓			✓		
	Suitable for MALDI sample preparation	✓	✓		✓							
Limitations	Require substrate modification	✓	✓	✓								✓
	Depends on particle shape							✓				
	Invasive (electric field)			✓								
	Invasive (chemical)			✓			✓					
	Invasive (heating)			✓	✓	✓						
	Require external forcing		✓	✓	✓						✓	

Fig. 8. Comparison of different methods. The working principle, advantages and limitations are illustrated.

or forming patterns of particles. In this section, we discuss such utilization of CRE.

3.1. Biochemical applications

Concentrating solutes at the rim of the droplet by CRE is called the self-ordered ring (SOR) method (Fig. 9a). It acts as a pre-concentration procedure before various analyses. Often a hydrophobic surface is used as the substrate in SOR method. Drying process on hydrophobic surfaces forms smaller rings with higher solute density as the contact line is pinned only in the later stages of the evaporation. Liu et al. demonstrated that the SOR method enhanced the fluorescence detection of orally administrated berberine in human urine [148]. Similarly, fluorescent detection of trace levels of tetracycline [149], quinidine sulfate in serum samples [150] and fluorescein [151] was demonstrated based on the SOR method.

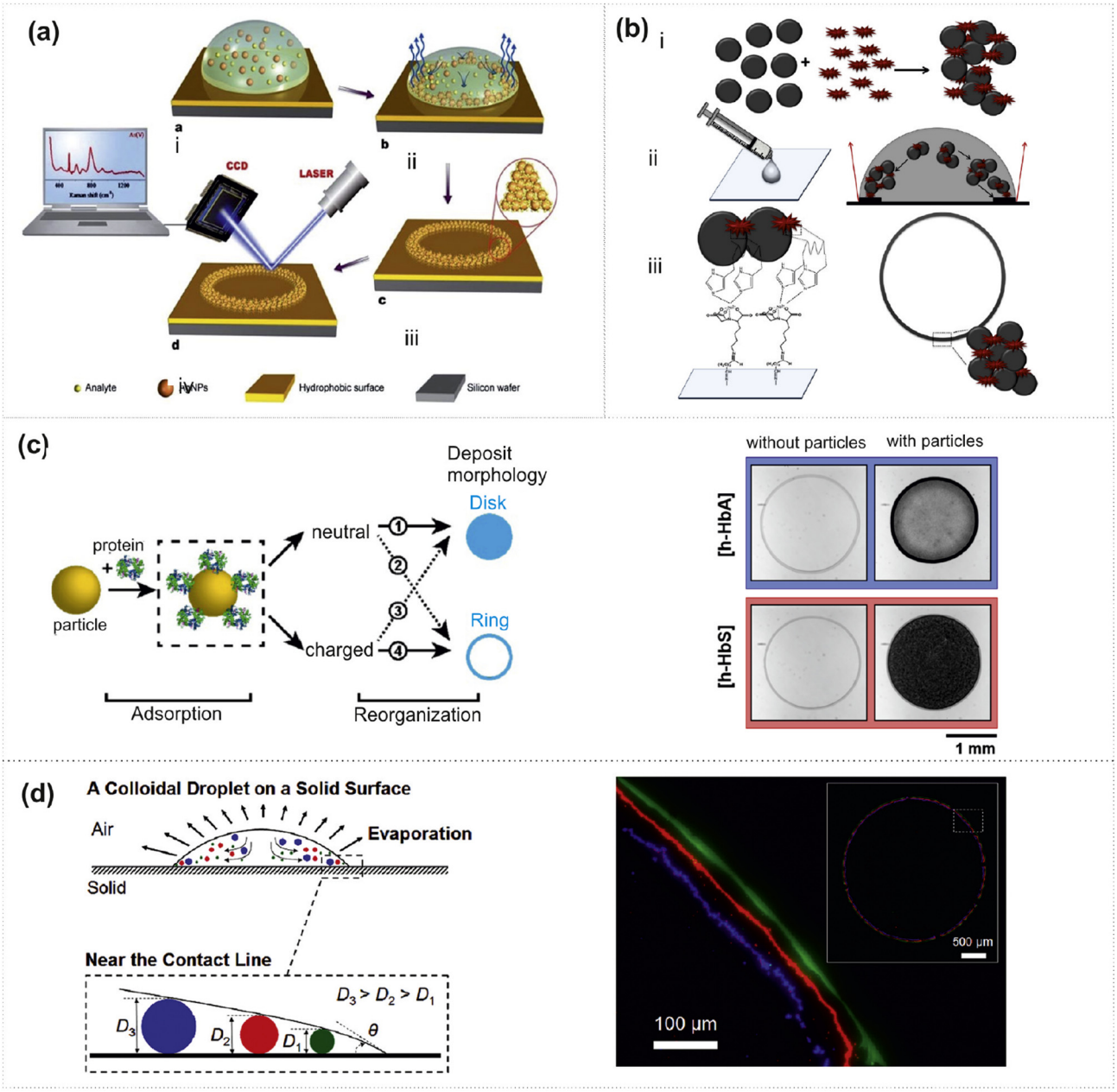

Fig. 9. The CRE is used as a beneficial effect in various applications. (a) The enhancement of the analyte concentration at the ring along with the Ag-nanoparticles improves detection by SERS. Adapted with permission from: [17] Copyright ©2014, Royal Society of Chemistry. (b) An immunoassay is demonstrated with a solution of Au coated polystyrene nanoparticles and *Plasmodium falciparum* biomarker. (ii–iii) When the droplet of this solution dries on a glass slide, the biomarker proteins are aggregated with the particles at the contact line, mimicking an enzyme-linked immunosorbent assay. Adapted with permission from: [21] Copyright ©2014, American Chemical Society. (c) The CRE detects mutated protein haemoglobin (h-HbS) from its native form (h-HbA) when blood is dried with dispersed polystyrene particles of different charge. (Left panel): the adsorption of proteins alter the charge of the particles influencing the deposit morphology (paths 1 and 4). The exposure to charged (path 2) and hydrophobic (path 3) moieties inverts the effect. (Right panel): there is a notable difference in the patterns formed with healthy and pathogenic form of haemoglobin with (right) and without (left) the presence of anionic polystyrene particles. Adapted with permission from: [164] Copyright ©2016, American Chemical Society. (d) (Left): The CRE is used for chromatography for size-dependent particle separation near the contact line. (Right): Optical fluorescence image showing the separation of 40 nm (green), 1 µm (red), and 2 µm (blue) particles after evaporation. Adapted with permission from: [22] Copyright ©2011, American Chemical Society.

Wen et al. developed an aptamer biosensor based on the enhanced solute concentration at the ring [20]. They detected α-thrombin in human serum and four-fold-diluted whole blood. The SOR method gave a lower limit sensitivity of detection of 2 ng/mL (54 pM) in serum, and 4 ng/mL (105 pM) in the blood. Similarly, a malaria diagnostic platform was also reported based on the SOR method to detect *Plasmodium falciparum* histidine-rich protein-II, which is a biomarker indicative of the *P. falciparum* parasite strain [21,152] (Fig. 9b). In this sensor, gold-plated and surface chemical-modified polystyrene microspheres bind with the protein and form a sandwiched assay with the glass substrate at the contact line. The ring formation allowed sensitive detection with the naked eye at protein concentrations as low as 10 pM [21].

When SOR method is used in the Raman analysis (Fig. 9a) it is known as the 'droplet coating deposition Raman', which has shown its advantages, for example, in proteomics [153–156]. In particular, in SERS the nanoparticle aggregates at the ring can serve as hot spots as the chemical constituents to be detected get packed there along with the particles. The CRE assisted SERS measurements [17,157] particularly, the detection of polycyclic aromatic hydrocarbons in river water [158] and glycated haemoglobin [159], which is a promising target for monitoring the long term history of diabetes, are successful examples.

The drying patterns of biological fluids can have applications in forensics and diagnostics. For example, blood droplets form characteristic patterns upon drying [19], which are interesting in forensics [160]. For example, shape of the dried blood droplets can reveal the angle and velocity of the 'deposition' on the wall. Similarly, the dried patterns of blood can also reveal information regarding the disease status. The diagnostic value of dried blood samples for early detection of cancer was identified by Bolen in 1942 itself [161,162]. Later, various other studies were performed to investigate the diagnostic potential of the pattern on dried blood droplets as reviewed by Chen et al. [163].

Recently, Devineau et al. demonstrated that the patterns of the blood mixed with polystyrene particles differ when there is a point mutation in the protein haemoglobin, i.e. variation from healthy form (h-HbA) to the mutant pathogenic form (h-HbS) (Fig. 9c) [164]. In the droplet, h-HbS adsorbed on to the anionic particles resulting their migration to the liquid/air interface by the exposure of the hydrophobic regions of the adsorbed protein. It resulted in the suppression of CRE whereas the particle-h-HbA combination formed a clear CRE. Similarly, Li et al. used the shape of the residue as a readout for detecting DNA hybridization [165]. They functionalized the surface of microparticles with single-stranded oligonucleotide probes. When the complementary target DNA was introduced, hybridization occurred, connecting multiple particles. Such aggregation of the particles distorted the meniscus surrounding them inducing long-range capillary attraction and eventually influenced the residue shape. This method demonstrated high specificity and could identify even a single mismatch of a nucleotide.

Trantum et al. demonstrated concept of a biosensor based on the Marangoni flow in an evaporating drop [166]. They detected the presence of M13 bacteriophage as a model target. Marangoni flow concentrated the aggregates of dispersed 1 μ m-diameter particles, which are surface functionalized with anti-M13 monoclonal antibodies, formed in the presence of the target. In the absence of the bacteriophage, the aggregation did not occur and the dispersed particles did not get concentrated at the center of the droplet. Measuring the size of the final spot using standard microscopy they achieved a limit-of-detection of approximately 100 fM. In this sensor, the choice of suitable substrate material is important as the direction of Marangoni flow depends on the relative thermal conductivity of the substrate and the liquid [35].

Separation of nanoparticles, micro-organisms and mammalian cells in a liquid droplet was demonstrated using the CRE [22]. When the particles or cells flow into the liquid wedge they get spatially distributed depending upon their size. This method has a separation resolution on the order of 100 nm and a dynamic range from 10 nm to a few tens of micrometers (Fig. 9d). A similar technique was demonstrated making use of the thermally driven strong Marangoni flow generated by heating the substrate [167]. The strong Marangoni flow pushes the particles well into the liquid wedge increasing the resolution of separation.

Yadav et al. used CRE for the encapsulation of gold nanoparticles in poly-3-hydroxybutyrate (PHB) matrix using inkjet printing [168]. Here, an aqueous solution of the gold nanoparticles was deposited on a PHB surface and allowed to dry. Another droplet of PHB was added on to the dried spot and the miscible nature of the PHB substrate and PHB droplet encapsulated the nanoparticles in PHB.

The pre-concentration of samples using SOR method is very cost effective and require no special equipment. It is highly useful in SERS and MALDI based sensors where dried sample are used for the analysis. Although the SOR method increases the sensitivity, a more sensitive detection can be achieved if one could suppress CRE to concentrate all the solute into a single spot. This idea was demonstrated in the case of MALDI analysis [13–15]. One major issue in the SOR method is the non-specific adsorption of the active components on the substrate surface. Adsorption will prevent the analytes from reaching the contact line. The adsorption is much pronounced on hydrophobic substrates. Suppression methods based on acoustics, Marangoni effect and interfacial effects that are independent of the wettability of the substrate are suitable for concentrating biological samples.

One another issue is the fact that nanoparticles or molecules can get trapped with the salt crystals in the bulk of the droplet preventing their concentration. It occurs especially in the drying of biological fluids. Trantum et al. overcame this issue by adding glycerol in the droplet, which prevented complete drying, thus avoided the salt crystallization [166]. Concentrating the solute much before the completion of the drying can prevent the interference of the salt crystals. A suitable method in this context is acoustic streaming [86]. Further investigations are required to optimize CRE based biosensing and chromatography especially in the presence of biological samples.

Diagnostics based on the pattern formation can detect the presence of bio-markers in biological fluids. However, this detection is qualitative to identify the presence or absence of a particular species. Further investigations can be performed to relate the patterns to quantitative amount of the species. Another possible area of study is the pattern of cracks formed on the residue of biological samples, for example, blood, to predict a disease state and its progression.

3.2. Industrial applications

Evaporative self-assembly by CRE can form patterns using micro- and nanoparticles as the building blocks. For example, ordered 3D structures of particles can be produced by evaporation for photonic applications [169,170]. These applications require good control over the self-assembly process. In this regard, Choi et al. demonstrated a finely controlled way of assembling 3D structures of silica, metal oxide (TiO_2, ZnO) and metallic nanoparticles [171] (Fig. 10a, b). Here, CRE drives particles into the photo-patterned rectangular wells and trenches on the substrate. Various patterns are formed by adjusting the concentration and size of the particles in the solution. After the particle deposition in the wells or trenches the photoresist is removed to obtain the defined patterns.

The CRE was used to fabricate rings of synthesized mesoporous particles. The porous property of these particles was used for absorbing fluorescent dye for sensing applications [172]. Combination of CRE with dielectrophoresis was demonstrated to produce concentric patterns of polystyrene and TiO_2 nanoparticles [173]. Here, concentric electrodes patterned on the substrate were used to apply

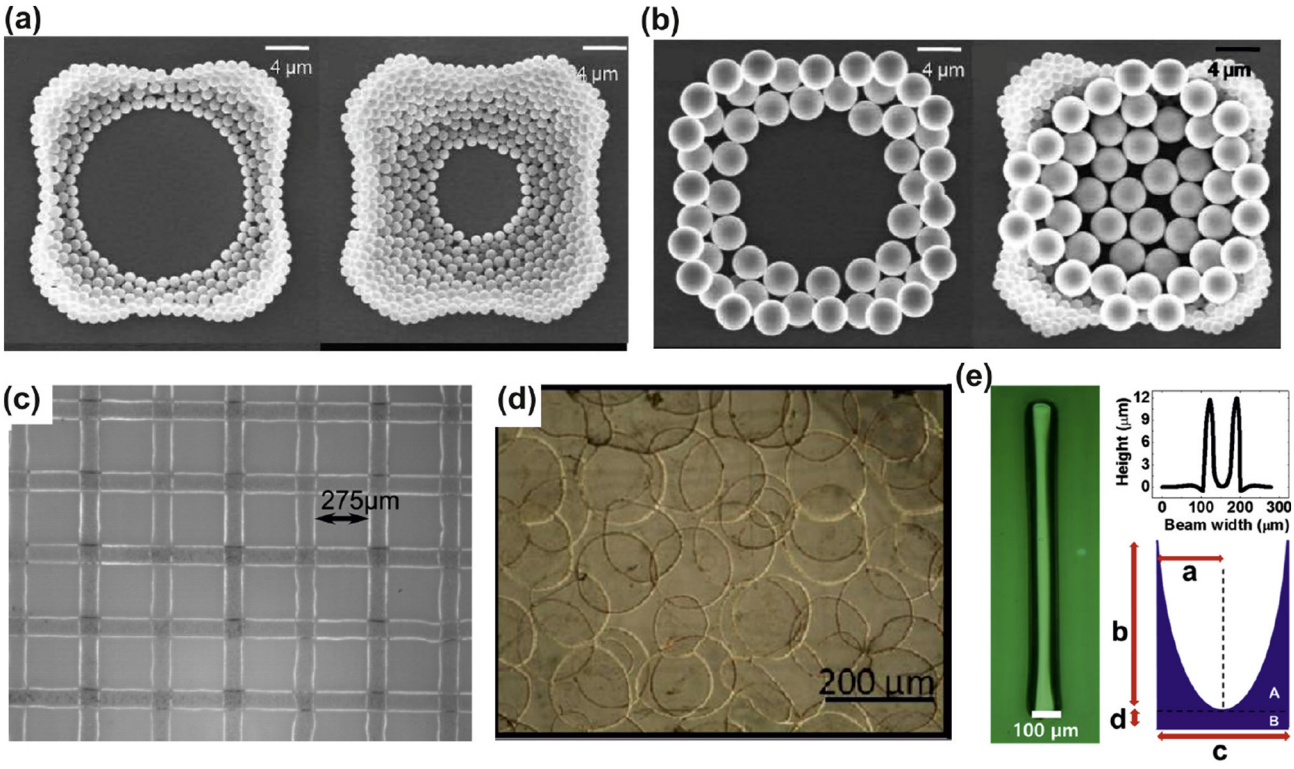

Fig. 10. CRE based patterning of particles. (a) Patterns of silica particles 1 μm. (b) Patterns with particles of two different diameters (1 and 3 μm). Adapted with permission from: [171] Copyright ©2010, American Chemical Society. (c) Optical image of a grid of conducting twin lines of silver nanoparticles. Adapted with permission from: [177] Copyright ©2013, American Physical Society. (d) An array of interconnected rings of silver nanoparticles acts as transparent conductive coating. Adapted with permission from: [179] Copyright ©2009, American Chemical Society. (e) Optical image, surface profile, and schematic cross-section of a cantilever strengthened by printed silver nanoparticles. Adapted with permission from: [183] Copyright ©2014, American Physical Society.

AC signal (0.1–100 Hz and 5 V) during the evaporation of the droplet. The spacing of the concentric rings and the patterned areas depended on the frequencies of the applied AC signal and the direction of the dielectrophoretic force. This force is negative and positive for polystyrene (PS) and TiO_2 particles, respectively.

The CRE was utilized in electronics applications, for example, to define channels in the fabrication of metal oxide thin-film transistors [174] and make high resolution patterns such as conductive wires of nanoparticles [8,175-178] (Fig. 10c). Such simple inkjet printing based methods can avoid complex lithographic steps and produce lines as thin as 5–10 μ m. Transparent conductive coatings were also fabricated based CRE [179]. These coatings consisted of 2D array of interconnected ring-like deposits of silver nanoparticles (Fig. 10d). The individual rings had a diameter of about 150 μ m, which were obtained by drying inkjet printed droplets [179]. Parallel twin conducting lines were fabricated by drying a ribbon-like droplet formed by a series of inkjet printed droplets containing silver nanoparticles [177,178] and multi-walled carbon nanotubes [180].

Ma et al. produced twin lines of particles by evaporation combined with a technique called *electroless* plating to adhere the particle reaching at the contact line to the substrate. The electroless plating uses a solution of metal salt, reducing agent, a complexing agent, and additives. The metal nucleates on the catalytically active surface producing strong bond between the surface and the metal particles. They inkjet printed the aqueous solution of poly(dopamine) silver nanoparticles on glass substrate to form twin lines followed by its immersion into silver nitrate solution for electroless plating [178].

Using CRE, Khapli et al. demonstrated fabrication of porous films [181] and scaffolds [182] from a wide variety of ceramic materials such as $CaCO_3$, ZnO, CuO, Co_3O_4, Co-doped ZnO and Ag_2O. This method consisted of evaporation of CO_2-enriched water microdroplets onto substrates heated to 120 °C. The $CaCO_3$ scaffolds have use in enhancing bone healing around titanium implants.

In an another interesting experiment, CRE was used for fabricating U-bar shaped micro-cantilevers [183] (Fig. 10e). It is difficult to fabricate curved surfaces using conventional microfabrication techniques. Due to CRE the inkjet printed silver nanoparticles formed thicker edges on the bar increasing its effective stiffness. Tuning the drying conditions the height of the edges can be controlled.

Self-assembly of particles by CRE is a cheap and simple method to fabricate photonic crystals and conducting wires. The self-assembly process depends strongly on the evaporation rate resulting in square, hexagonal and random ordering of the particles [32]. Slow evaporation deposits particles at a slow rate allowing them enough time to form ordered structures. However, fast evaporation rushes the particles to the contact line depositing them in an orderless fashion. Methods using surface templates, for example, as shown by Choi et al. can produce patterns having well defined edges.

When the particles are of higher density compared to the liquid, they may sink directly on to the surface of the substrate before reaching at the contact line. This scenario can result in a spread of the particles on the surface rather than thin lines. However, this difficulty can be overcome by tuning the evaporation rate and using small particles (say, nanoparticles). In general, controlling the evaporation rate, liquid properties (such as density and composition) and substrate wettability help formation of thin wire-like patterns of particles. When the deposition process is well optimized the particles tightly assemble at the contact line forming a conductive wire even without additional processing for example thermal sintering. However, thermal sintering can improve the quality by

connecting the particles firmly avoiding cracks and thus making the wires robust [175,177]. Thermal sintering is not compatible when the wires need to be produced on polymer substrates. The method developed by Zhang et al. could pattern wires on flexible poly(ethyleneterephthalate) substrates with a sintering process at room temperature [176]. CRE combined with electroless plating is a suitable method to pattern strong wires on flexible substrates [178], where no thermal treatments are required.

A control over the evaporative deposition process is necessary to design new patterns and fine tune them. For example, controlled evaporation of polymer solutions has produced well defined concentric gradient rings [184–187]. Here, the control was achieved by using microparticles as templates or capillary bridges in confined geometries composed of either two cylindrical mica surfaces placed perpendicular to one another [185] or a sphere placed on flat surface [186,187].

A dynamic control over the deposition process can give more options to tune the patterns. Dynamic control of the deposition process can be achieved by using the same methods used for the suppression of CRE, such as electrowetting, electroosmotic flow, laser irradiation and acoustics. Turning the external forcing *on* and *off* during the evaporation, a positive and negative feedback in the deposition process can be induced. Acoustics based method offers an additional capability for preferential control over the particles being deposited based on their size. Such a dynamic control of the CRE is not possible in methods involving modification of the solvent or the solute.

4. Summary

This review summarizes various strategies related to suppression and utilization of CRE. We have highlighted scientific and technological developments initiated by the rich physical phenomena involved in CRE. The curiosity driven scientific studies aimed at understanding of CRE and the application-motivated studies focusing on how to avoid CRE have given rise to novel manufacturing approaches. We believe emerging challenges highlighted in Section "Advantages and Limitation", particularly with strongly pinning nanomaterials, offer promising research directions.

On the other hand, CRE inspired approaches can be utilized to improve biochemical analyses and prepare new materials through convection induced assembly. In biochemical analyses, CRE enables concentration of analytes by making use of contact line pinning and capillary flows. Similarly, ordered colloidal structures can be constructed through convection induced self-assembly at the contact line. We have described existing challenges and suggested possible directions for future research at the end of each sections.

Acknowledgments

The authors acknowledges Dr. Sajan Daniel George and Eric Reza Safai for valuable comments. DM acknowledges SERB (India) grant (30216008) and HBE acknowledges Veni grant from NWO.

References

[1] Larson RG. Re-shaping the coffee ring. Angew Chem 2012;51:2546–8.
[2] Larson RG. Transport and deposition patterns in drying sessile droplets. AIChE J 2014;60:1538–71.
[3] Ma H, Hao J. Ordered patterns superlattices, honeycomb structures and coffee rings. Chem Soc Rev 2011;40:5457–71.
[4] Deegan RD, Bakajin O, Dupont TF, Huber G, Nagel SR, Witten TA. Capillary flow as the cause of ring stains from dried liquid drops. Nature 1997;389:827–9.
[5] Hu H, Larson RG. Evaporation of a sessile droplet on a substrate. J Phys Chem B 2002;106:1334–44.
[6] Park J, Moon J. Control of colloidal particle deposit patterns within picoliter droplets ejected by ink-jet printing. Langmuir 2006;22:3506–13.
[7] Friederich A, Binder JR, Bauer W. Rheological control of the coffee stain effect for inkjet printing of ceramics. J Am Ceram Soc 2013;96:2093–9.
[8] Kuang M, Wang L, Song Y. Controllable printing droplets for high-resolution patterns. Adv Mater 2014;26:6950–8.
[9] Sun J, Bao B, He M, Zhou H, Song Y. Recent advances in controlling the depositing morphologies of inkjet droplets. ACS Appl Mater Interfaces 2015;7:28086–99.
[10] Blossey R, Bosio A. Contact line deposits on cDNA microarrays: a "twin-spot effect". Langmuir 2002;18:2952–4.
[11] Dugas V, Broutin J, Souteyrand E. Droplet evaporation study applied to DNA chip manufacturing. Langmuir 2005;21:9130–6.
[12] Hu JB, Chen YC, Urban PL. Coffee-Ring effects in laser desorption/ionization mass spectrometry. Anal Chim Acta 2013;766:77–82.
[13] Mampallil D, Eral HB, van den Ende D, Mugele F. Control of evaporating complex fluids through electrowetting. Soft Matter 2012;8:10614–7.
[14] Kudina O, Eral B, Mugele F. E-MALDI: an electrowetting-enhanced drop drying method for MALDI mass spectrometry. Anal Chem 2016;88:4669–75.
[15] Lai YH, Cai YH, Lee H, Ou YM, Hsiao CH, Tsao CW. et al. Reducing spatial heterogeneity of MALDI samples with Marangoni flows during sample preparation. J Am Soc Mass Spectrom 2016;27:1314–21.
[16] Zhou W, Hu A, Bai S, Ma Y, Su Q. Surface-enhanced Raman spectra of medicines with large-scale self-assembled silver nanoparticle films based on the modified coffee ring effect. Nanoscale Res Lett 2014;9:87.
[17] Wang W, Yin Y, Tana Z, Liu J. Coffee-ring effect-based simultaneous SERS substrate fabrication and analyte enrichment for trace analysis. Nanoscale 2014;6:9588–93.
[18] Li P, Li Y, Zhou ZK, Tang S, Yu XF, Xiao S. et al. Evaporative self-assembly of gold nanorods into macroscopic 3D plasmonic superlattice arrays. Adv Mat 2016;28:2511–7.
[19] Brutin D, Sobac B, Loquet B, Sampol J. Pattern formation in drying drops of blood. J Fluid Mech 2011;667:85–95.
[20] Wen JT, Ho CM, Lillehoj PB. Coffee ring aptasensor for rapid protein detection. Langmuir 2013;29:8440–6.
[21] Gulka CP, Swartz JD, Trantum JR, Davis KM, Peak CM, Denton AJ. et al. Coffee rings as low-resource diagnostics: detection of the malaria biomarker *Plasmodium falciparum* histidine-rich protein-II using a surface-coupled ring of ni(II)NTA gold-plated polystyrene particles ACS. Appl Mater Interfaces 2014;6:6257–63.
[22] Wong TS, Chen TH, Shen X, Ho CM. Nanochromatography driven by the coffee ring effect. Anal Chem 2011;83:1871–3.
[23] de Gans BJ, Schubert US. Inkjet printing of well-defined polymer dots and arrays. Langmuir 2004;20:7789–93.
[24] Han W, Lin Z. Learning from "coffee-rings": ordered structures enabled by controlled evaporative self-assembly. Angew Chem Int Ed 2012;51:1534–46.
[25] Shao JJ, Lv W, Yang QH. Self-assembly of graphene oxide at interfaces. Adv Mat 2014;26:5586.
[26] Zou J, Kim F. Diffusion driven layer-by-layer assembly of graphene oxide nanosheets into porous three-dimensional macrostructures. Nat Commun 2014;5:5254.
[27] Park J, Moon J, Shin H, Wang D, Park M. Direct-write fabrication of colloidal photonic crystal microarrays by ink-jet printing. Colloid Interf. Sci. 2006;298:713–9.
[28] Cui L, Li Y, Wang J, Tian E, Zhang X, Zhang Y. et al. Fabrication of large-area patterned photonic crystals by ink-jet printing. J Mater Chem 2009;19:5499–502.
[29] Parisse F, Allain C. Shape changes of colloidal suspension droplets during drying. J Phys 1996;II(6):1111–9.
[30] Parisse F, Allain C. Drying of colloidal suspension droplets: experimental study and profile renormalization. Langmuir 1997;13:3598–602.
[31] Deegan R, Bakajin O, Dupont TF, Huber G, Nagel SR, Witten TA. Contact line deposits in an evaporating drop. Phys Rev E 2000;62:756.
[32] Marín AG, Gelderblom H, Lohse D, Snoeijer JH. Order-to-disorder transition in ring-shaped colloidal stains. Phys Rev Lett 2011;107:085502.
[33] Das S, Chakraborty S, Mitra SK. Ring stains in the presence of electrokinetic interactions. Phys Rev E 2012;85:046311.
[34] Davis SH. Thermocapillary instabilities. Annu Rev Fluid Mech 1987;19:403.
[35] Ristenpart WD, Kim PG, Domingues C, Wan J, Stone HA. Influence of substrate conductivity on circulation reversal in evaporating drops. Phys Rev Lett 2007;99:234502.
[36] Bhardwaj R, Fang X, Somasundaran P, Attinger D. Self-assembly of colloidal particles from evaporating droplets: role of DLVO interactions and proposition of a phase diagram. Langmuir 2010;26:7833–42.
[37] Yunker PJ, Lohr MA, Still T, Borodin A, Durian DJ, Yodh AG. Effects of particle shape on growth dynamics at edges of evaporating drops of colloidal suspensions. Phys Rev Lett 2013;110:035501.
[38] Sacanna S, Pine DJ, Yi GR. Engineering shape: the novel geometries of colloidal self-assembly. Soft Matter 2013;9:8096–106.
[39] Weon BM, Je JH. Capillary force repels coffee-ring effect. Phys Rev E 2010;82:015305(R).
[40] Manoharan VN, Elsesser MT, Pine DJ. Dense packing and symmetry in small clusters of microspheres. Science 2003;301:483–7.
[41] Lauga E, Brenner MP. Evaporation-driven assembly of colloidal particles. Phys Rev Lett 2004;93:238301.
[42] Popov YO. Evaporative deposition patterns spatial dimensions of the deposit. Phys Rev E 2005;71:036313.

[43] Craster RV, Matar OK, Sefiane K. Pinning, retraction, and terracing of evaporating droplets containing nanoparticles. Langmuir 2009;25:3601–9.
[44] Witten TA. Robust fadeout profile of an evaporation stain. Europhys Lett 2009;86:
[45] Freed-Brown J. Evaporative deposition in receding drops. Soft Matter 2014;10:9506–10.
[46] Man X, Doi M. Ring to mountain transition in deposition pattern of drying droplets. Phys Rev Lett 2016;116:066101.
[47] Fischer BJ. Particle convection in an evaporating colloidal droplet. Langmuir 2002;18:60–7.
[48] Ozawa K, Nishitani E, Doi M. Modeling of the drying process of liquid droplet to form thin film. Jpn JAppl Phys 2005;44:4229.
[49] Okuzono T, Kobayashi M, Doi M. Final shape of a drying thin film. Phys Rev E 2009;80:021603.
[50] Eales AD, Routh AF, Dartnell N, Goddard S. Evaporation of pinned droplets containing polymer — an examination of the important groups controlling final shape. Transp Phenom Fluid Mech 2015;61:1759–67.
[51] Eales AD, Dartnell N, Goddard S, Routh AF. The impact of trough geometry on film shape. A theoretical study of droplets containing polymer, for p-OLED display applications. J Colloid Interface Sci 2015;458:53–61.
[52] Karapetsas G, Sahu KC, Matar OK. Evaporation of sessile droplets laden with particles and insoluble surfactants. Langmuir 2016;32:6871–81.
[53] Frastia L, Archer AJ, Thiele U. Dynamical model for the formation of patterned deposits at receding contact lines. Phys Rev Lett 2011;106:077801.
[54] Fraštia L, Archer AJ, Thiele U. Modelling the formation of structured deposits at receding contact lines of evaporating solutions and suspensions. Soft Matter 2012;8:11363–86.
[55] Kaplan C, Mahadevan L. Evaporation-driven ring and film deposition from colloidal droplets. J of Fluid Mech 2015;781:R2.
[56] Shen X, Ho CM, Wong TS. Minimal size of coffee ring structure. J Phys Chem B 2010;114:5269–74.
[57] De Gennes, Wetting PG. Statics and dynamics. Rev Mod Phys 1985;57:827–63.
[58] Bonn D, Eggers J, Indekeu J, Meunier J, Rolley E. Wetting and spreading. Rev Modern Phys 2009;81:739–804.
[59] Eral HB, 't Mannetje DJCM, Oh JM. Contact angle hysteresis: a review of fundamentals and applications. Colloid Polym Sci 2013;291:247–60.
[60] Anyfantakis M, Baigl D. Manipulating the coffee-ring effect: interactions at work. ChemPhysChem 2015;16:2726–34.
[61] Ko HY, Park J, Shin H, Moon J. Rapid self-assembly of monodisperse colloidal spheres in an ink-Jet printed droplet. Chem Mater 2004;16:4212–5.
[62] Tian D, Song Y, Jiang L. Patterning of controllable surface wettability for printing techniques. Chem Soc Rev 2013;42:5184–209.
[63] Semprebon C, McHale G, Kusumaatmaja H. Re-shaping the coffee ring. Soft matter 2017;13,1:101–10.
[64] Chen L, Evans JR. Drying of colloidal droplets on superhydrophobic surfaces. J Colloid Interface Sci 2010;351:283–7.
[65] Brunet P. Particle deposition after droplet evaporation on ultra-hydrophobic micro-textured surfaces. Soft Matter 2012;8:11294–301.
[66] Ta VD, Dunn A, Wasley TJ, Li J, Kay RW, Stringer J. et al. Laser textured superhydrophobic surfaces and their applications for homogeneous spot deposition. Appl Surf Sci 2016;365:153–9.
[67] Marín AG, Gelderblom H, Susarrey-Arce A, van Houselt A, Lefferts L, Gardeniers JG. et al. Building microscopic soccer balls with evaporating colloidal fakir drops. Proc Natl Acad Sci U S A 2012;109:16455–8.
[68] Dicuangco M, Dash S, Weibel JA, Garimella SV. Effect of superhydrophobic surface morphology on evaporative deposition patterns. Appl Phys Lett 2014;104:201604.
[69] Semprebon C, Forsberg P, Priest C, Brinkmann M. Pinning and wicking in regular pillar arrays. Soft Matter 2014;10:5739.
[70] Cui L, Zhang J, Zhang X, Li Y, Wang Z, Gao H. et al. Avoiding coffee ring structure based on hydrophobic silicon pillar arrays during single-drop evaporation. Soft Matter 2012;8:10448–56.
[71] Dai X, Stogin BB, Yang S, Wong TS. Slippery Wenzel state. ACS Nano 2015;9:9260–7.
[72] Moraila-Martinez CL, Cabrerizo-Vilchez MA, Rodriguez-Valverde MA. Controlling the morphology of ring-like deposits by varying the pinning time of driven receding contact lines. Interfacial Phenom Heat Transfer 2013;1:195–205.
[73] Nguyen TAH, Hampton MA, Nguyen AV. Evaporation of nanoparticle droplets on smooth hydrophobic surfaces: the inner coffee ring deposits. J Phys Chem C 2013;117:4707–16.
[74] Li F, Sheng YJ, Tsao HK. Evaporation stains. Langmuir 2013;29:7802–11.
[75] Mugele F, Baret JC. Electrowetting: from basics to applications. J Phys Condens Matter 2005;17:R705.
[76] Li F, Mugele F. How to make sticky surfaces slippery: contact angle hysteresis in electrowetting with alternating voltage. Appl Phys Lett 2008;92:244108.
[77] Eral HB, Augustine DM, Duits MHG, Mugele F. Suppressing the coffee stain effect: how to control colloidal self-assembly in evaporating drops using electrowetting. Soft Matter 2011;7:4954–8.
[78] Wray AW, Papageorgiou DT, Craster RV, Sefiane K, Matar OK. Electrostatic suppression of the "coffee stain effect". Langmuir 2014;30:5849–58.
[79] Zhang J, Borg MK, Ritos K, Reese JM. Electrowetting controls the deposit patterns of evaporated salt water nanodroplets. Langmuir 2016;32:1542–9.
[80] Kim SJ, Kang KH, Lee JG, Kang IS, Yoon BJ. Control of particle-deposition pattern in a sessile droplet by using radial electroosmotic flow. Anal Chem 2006;78:5192–7.
[81] Muangnapoh T, Weldon AL, Gilchrist JF. Enhanced colloidal monolayer assembly via vibration-assisted convective deposition. Appl Phys Lett 2013;103:181603.
[82] Zabihi F, Eslamian M. Substrate vibration-assisted spray coating (SVASC): significant improvement in nano-structure, uniformity, and conductivity of PEDOT:PSS thin films for organic solar cells. J Coat Technol Res 2015;12:711–9.
[83] Yeo LY, Friend JR. Surface acoustic wave microfluidics annu. Rev Fluid Mech 2014;46:379–406.
[84] Mampallil D, Reboud J, Wilson R, Wylie D, Klug DR, Cooper JM. Acoustic suppression of the coffee-ring effect. Soft Matter 2015;11:7207–13.
[85] Mhatre S, Zigelman A, Abezgauz L, Manor O. Influence of a propagating megahertz surface acoustic wave on the pattern deposition of solute mass off an evaporating solution Langmuir, DOI: 10.1021/acs.langmuir.6b01341.
[86] Mampallil D, Reboud J, Wilson R, Cooper JM. 18Th international conference on miniaturized systems for chemistry and life sciences.2014.San Antonio, Texas, USA. p1193 October 26-30.
[87] Nguyen VX, Stebe KJ. Patterning of small particles by a surfactant-enhanced Marangoni-Bénard instability. Phys Rev Lett 2002;88:164501-4.
[88] Hu H, Larson RG. Analysis of the effects of Marangoni stresses on the microflow in an evaporating sessile droplet. Langmuir 2005;21:3972–80.
[89] Deegan RD. Pattern formation in drying drops. Phys Rev E 2000;61:475.
[90] Hu H, Larson RG. Marangoni effect reverses coffee-ring depositions. J Phys Chem B 2006;110:7090–4.
[91] Hendarto E, Gianchandani YB. Size sorting of floating spheres based on Marangoni forces in evaporating droplets. J Micromech Microeng 2013;23:075016.
[92] Li Y, Lv C, Li Z, Quéré D, Zheng Q. From coffee rings to coffee eyes. Soft Matter 2015;11:4669–73.
[93] Parsa M, Harmand S, Sefiane K, Bigerelle M, Deltombe R. Effect of substrate temperature on pattern formation of nanoparticles from volatile drops. Langmuir 2015;31:3354–67.
[94] Ta VD, Carter RM, Esenturk E, Connaughton C, Wasley TJ, Li J. et al. Dynamically controlled deposition of colloidal nanoparticle suspension in evaporating drops using laser radiation. Soft Matter 2016;12:4530–6.
[95] Lim JA, Lee WH, Lee HS, Lee JH, Park YD, Cho K. Self-organization of ink–jet-printed triisopropylsilylethynyl pentacene via evaporation-induced flows in a drying droplet. Adv Funct Mater 2008;18:229–34.
[96] Talbot EL, Berson A, Bain CD. NIP28: 28th international conference on digital printing technologies and digital fabrication, Quebec City, Canada. The Society for Imaging Science and Technology: Springfield, VA.; 2012,420–3.
[97] Seo C, Jang D, Chae J, Shin S. Altering the coffee-ring effect by adding a surfactant-like viscous polymer solution. Sci Rep 2017;7:
[98] Zhong X, Duan F. Flow regime and deposition pattern of evaporating binary mixture droplet suspended with particles. Eur Phys J E 2016;39:18.
[99] Jin H, Qian J, Zhou L, Yuan J, Huang H, Wang Y. et al. Suppressing the coffee-ring effect in semitransparent MnO_2 film for a high-performance solar-powered energy storage window. ACS Appl Mater Interfaces 2016;8:9088–96.
[100] Still T, Yunker PJ, Yodh AG. Surfactant-induced marazngoni eddies alter the coffee-rings of evaporating colloidal drops. Langmuir 2012;28:4984–8.
[101] Erbil HY. Control of stain geometry by drop evaporation of surfactant containing dispersions. Adv Colloid Interf Sci 2015;222:275–90.
[102] Sempels W, Dier RD, Mizuno H, Hofkens J, Vermant J. Auto-production of biosurfactants reverses the coffee ring effect in a bacterial system. Nat Commun 2013;4:1757.
[103] Marin A, Liepelt R, Rossi M, Kähler CJ. Surfactant-driven flow transitions in evaporating droplets. Soft Matter 2016;12:1593–600.
[104] Michen B, Geers C, Vanhecke D, Endes C, Rothen-Rutishauser B, Balog S. et al. Avoiding drying-artifacts in transmission electron microscopy: characterizing the size and colloidal state of nanoparticles. Sci Rep 2015;5:9793.
[105] Majumder M, Rendall CS, Eukel JA, Wang JYL, Behabtu N, Pint CL. et al. Overcoming the "coffee-stain" effect by compositional Marangoni-flow-assisted drop-drying. J Phys Chem B 2012;116:6536.
[106] Crivoi A, Duan F. Attenuating the coffee-ring effect in drying sessile nanofluid droplets. Phys Rev Amplif. E 2013;87:042303.
[107] Crivoi A, Duan F. Elimination of the coffee-ring effect by promoting particle adsorption and long-range interaction. Langmuir 2013;29:12067–74.
[108] Crivoi A, Zhong X, Duan F. Crossover from the coffee-ring effect to the uniform deposit caused by irreversible cluster-cluster aggregation. Phys Rev E 2015;92:032302.
[109] Dugyala VR, Basavaraj MG. Control over coffee-ring formation in evaporating liquid drops containing ellipsoids. Langmuir 2014;30:8680–6.
[110] Choi S, Pisano AP, Zohdi TI. An analysis of evaporative self-assembly of micro particles in printed picoliter suspension droplets. Thin Solid Films 2013;537:180–9.
[111] Dugyala VR, Basavaraj MG. Evaporation of sessile drops containing colloidal rods: coffee-ring and order-disorder transition. J Phys Chem B 2015;119:3860–7.
[112] Fleury B, Dantelle G, Darbe S, Boilot JP, Gacoin T. Transparent coatings made from spray deposited colloidal suspensions. Langmuir 2012;28:7639–45.
[113] Tang Y, He W, Wang S, Tao Z, Cheng L. The superiority of silver nanoellipsoids synthesized via a new approach in suppressing the coffee-ring effect during drying and film formation processes. Nanotechnology 2014;25:125602.
[114] Sun P, Ma R, Wang K, Zhong M, Wei J, Wu D. Suppression of the coffee-ring effect by self-assembling graphene oxide and monolayer titania. Nanotechnology 2013;24:075601.

[115] Morales VL, Parlange JY, Wu M, Pérez-Reche FJ, Zhang W, Sang W. Surfactant-mediated control of colloid pattern assembly and attachment strength in evaporating droplets. Langmuir 2013;29:1831–40.
[116] Stamou D, Duschl C, Johannsmann D. Long-range attraction between colloidal spheres at the air-water interface: the consequence of an irregular meniscus. Phys Rev E 2000;62:5263.
[117] Dasgupta S, Katava M, Faraj M, Auth T, Gompper G. Capillary assembly of microscale ellipsoidal, cuboidal, and spherical particles at interfaces. Langmuir 2014;30:11873–82.
[118] Yunker PJ, Still T, Lohr MA, Yodh AG. Suppression of the coffee-ring effect by shape-dependent capillary interactions. Nature 2011;476:308–11.
[119] Léandri J, Würger A. Trapping energy of a spherical particle on a curved liquid interface. J Colloid Interface Sci 2013;405:249–55.
[120] Yan Q, Gao L, Sharma V, Chiang YM, Wong CC. Particle and substrate charge effects on colloidal self-assembly in a sessile drop. Langmuir 2008;24:11518–22.
[121] Anyfantakis M, Geng Z, Morel M, Rudiuk S, Baigl D. Modulation of the coffee-ring effect in particle/surfactant mixtures: the importance of particle-interface interactions. Langmuir 2015;31:4113–20.
[122] Horigome K, Suzuki D. Drying mechanism of poly(n-isopropylacrylamide) microgel dispersions. Langmuir 2012;28:12962–70.
[123] Still T, Yunker PJ, Hanson K, Davidson ZS, Lohr MA, Aptowicz KB. et al. Hydrogels: temperature-sensitive hydrogel-particle films from evaporating drops. Adv Mater Interfaces 2015;2. https://doi.org/10.1002/admi.201570078.
[124] Zhang J, Pelton R. Poly(n-isopropylacrylamide) microgels at the air-water interface. Langmuir 1999;15:8032–6.
[125] Anyfantakis M, Baigl D. Dynamic photocontrol of the coffee-ring effect with optically tunable particle stickiness. Angew Chem Int Ed Engl 2014;53:14077–81.
[126] Bigioni TP, Lin XM, Nguyen TT, Corwin EI, Witten TA, Jaeger HM. Kinetically driven self assembly of highly ordered nanoparticle monolayers. Nat Mater 2006;5:265–70.
[127] Li Y, Yang Q, Li M, Song Y. Rate-dependent interface capture beyond the coffee-ring effect. Sci Rep 2016;6:24628.
[128] Talbot EL, Yang L, Berson A, Bain CD. Control of the particle distribution in inkjet printing through an evaporation-driven sol-gel transition. ACS Appl Mater Interfaces 2014;6:9572–83.
[129] Talbot EL, Yow HN, Yang L, Berson A, Biggs SR, Bain CD. Printing small dots from large drops. ACS Appl Mater Interfaces 2015;7:3782–90.
[130] Kajiya T, Kobayashi W, Okuzono T, Doi M. Controlling the drying and film formation processes of polymer solution droplets with addition of small amount of surfactants. J Phys Chem B 2009;113:15460–6.
[131] Cui L, Zhang J, Zhang X, Huang L, Wang Z, Li Y. et al. Suppression of the coffee ring effect by hydrosoluble polymer additives. ACS Appl Mater Interfaces 2012;4:2775–80.
[132] Msambwa Y, Shackleford ASD, Ouali FF, Fairhursta DJ. Controlling and characterising the deposits from polymer droplets containing microparticles and salt. Eur Phys J E 2016;39:21.
[133] Cui LY, Yan Y, Zhao XY, Yu CL, Ma Y, Yang B. et al. Controlling coffee ring structure on hydrophobic polymer surface by manipulating wettability with O_2 plasma. Chin Chem Lett 2016; https://doi.org/10.1016/j.cclet.2016.07.028.
[134] Biswas N, Datta A. Coffee-ring patterns of polymer droplets. AIP Conf Proc 2013;1512:142.
[135] Wang L, Wang J, Huang Y, Liu M, Kuang M, Li Y. Inkjet Printed colloidal photonic crystal microdot with fast response induced by hydrophobic transition of poly(N-isopropyl acrylamide). J Mater Chem 2012;22:21405.
[136] van den Berg AMJ, de Laat AW, Smith PJ, Perelaer J, Schubert US. Geometric control of inkjet printed features using a gelating polymer. J Mater Chem 2007;17:677–83.
[137] Soltman D, Subramanian V. Inkjet-printed line morphologies and temperature control of the coffee ring effect. Langmuir 2008;24:2224–31.
[138] Gorr HM, Zueger JM, Barnard JA. Lysozyme pattern formation in evaporating drops. Langmuir 2012;28:4039–42.
[139] Pack M, Hu H, Kim DO, Yang X, Sun Y. Colloidal drop deposition on porous substrates: competition among particle motion, evaporation, and infiltration. Langmuir 2015;31:7953–61.
[140] Nilghaz A, Zhang L, Shen W. Coffee stains on paper. Chem Eng Sci 2015;129:34–41.
[141] Kajiya T, Kobayashi W, Okuzono T, Doi M. Controlling profiles of polymer dots by switching between evaporation and condensation. Langmuir 2010;26:10429–32.
[142] Eales AD, Routh AF. Elimination of coffee-ring formation by humidity cycling: a numerical study. Langmuir 2016;32:505–11.
[143] Schirmer NC, Ströhle S, Tiwari MK, Poulikakos D. On the principles of printing sub-micrometer 3D structures from dielectric-liquid-based colloids. Adv Funct Mater 2011;21:388–95.
[144] Du X, Deegan RD. Ring formation on an inclined surface. J Fluid Mech 2015;775:R3.
[145] Zhou W, Hu A, Bai S, Ma Y, Bridges D. Anisotropic optical properties of large-scale aligned silver nanowire films via controlled coffee ring effects. RSC Adv 2015;5:39103–9.
[146] Hernandez-Perez R, Fan ZH, Garcia-Cordero JL. Evaporation-driven bioassays in suspended droplets. Anal Chem 2016;88:7312–7.
[147] Angelis FD, Gentile F, Mecarini F, Das G, Moretti M, Candeloro P. et al. Breaking the diffusion limit with super-hydrophobic delivery of molecules to plasmonic nanofocusing SERS structures. Nat Photonics 2011;5:682–7.
[148] Liu Y, Huang CZ, Li YF. Fluorescence assay based on preconcentration by a self-ordered ring using berberine as a model analyte. Anal Chem 2002;74:5564–8.
[149] Huang CZ, Liu Y, Li YF. Microscopic determination of tetracycline based on aluminum-sensitized fluorescence of a self-ordered ring formed by a sessile droplet on glass slide support. J Pharm Biomed Anal 2004;34:103–14.
[150] Yang C, Huang C. Fluorescent microscopic determination of quinidine sulfate in serum samples with self-ordered ring technique by capillary flow effect. Chin J Anal Chem 2006;34:183–7.
[151] Liu Y, Li YF, Huang CZ. Fluorimetric determination of fluorescein at the femtomole level with a self-ordered ring of a sessile droplet on glass slide support. J Anal Chem 2006;61:647–53.
[152] Trantum JR, Wright DW, Haselton FR. Biomarker-mediated disruption of coffee-ring formation as a low resource diagnostic indicator. Langmuir 2012;28:2187–93.
[153] Filik J, Stone N. Drop coating deposition Raman spectroscopy of protein mixtures. Analyst 2007;132:544–50.
[154] Zhang D, Xie Y, Mrozek MF, Ortiz C, Davisson VJ, Ben-Amotz D. Raman detection of proteomic analytes. Anal Chem 2003;75:5703–9.
[155] Ortiz C, Zhang D, Xie Y, Ribbe AE, Ben-Amotz D. Validation of the drop coating deposition Raman method for protein analysis. Anal Biochem 2006;353:157–66.
[156] Halvorson RA, Leng W, Vikesland PJ. Differentiation of microcystin, nodularin, and their component amino acids by drop-coating deposition raman spectroscopy. Anal Chem 2011;83:9273–80.
[157] Pan X, Dong J, Li Y, Sun X, Yuan C, Qian W. The strategy of two-scale interface enrichment for constructing ultrasensitive SERS substrates based on the coffee ring effect of agNP@β-CD. RSC Adv 2016;6:29586–91.
[158] Xu J, Du J, Jing C, Zhang Y, Cui J. Facile detection of polycyclic aromatic hydrocarbons by a surface-enhanced Raman scattering sensor based on the Au coffee ring effect. ACS Appl Mater Interfaces 2014;6:6891–7.
[159] Barman I, Dingari NC, Kang JW, Horowitz GL, Dasari RR, Feld MS. Raman spectroscopy-based sensitive and specific detection of glycated hemoglobin. Anal Chem 2012;84:2474–82.
[160] Attinger D, Moore C, Donaldson A, Jafari A, Stone HA. Fluid dynamics topics in bloodstain pattern analysis: comparative review and research opportunities. Forensic Sci Int 2013;231:375–96.
[161] Bolen HL. The blood pattern as a clue to the diagnosis of malignant disease. J Lab Clin Med 1942;27:1522–36.
[162] Bolen HL. Review of experience with the blood pattern test from 1939 to 1953. Am J Surg 1954;87:205–10.
[163] Chen R, Zhang L, Zang D, Shen W. Adv Colloid Interf Sci 2016;231:1–14.
[164] Devineau S, Anyfantakis M, Marichal L, Kiger L, Morel M, Rudiuk S. et al. Protein adsorption and reorganization on nanoparticles probed by the coffee-ring effect: application to single point mutation detection. J Am Chem Soc 2016;138:11623–32.
[165] Li Y, Zhao Z, Lam ML, Liu W, Yeung PP, Chieng CC. et al. Hybridization-induced suppression of coffee ring effect for nucleic acid detection. Sens Actuators B Chem 2015;206:56–64.
[166] Trantum jR, Baglia ML, Eagleton ZE, Mernaugh RL, Haselton FR. Biosensor design based on Marangoni flow in an evaporating drop. Lab Chip 2014;14:315–24.
[167] Jeong H, van Tiem J, Gianchandani YB, Park J. Nanoparticle separation using Marangoni flow in evaporating droplets. South Carolina: Hilton Head Island; 2014.
[168] Yadav R, Balasubramanian K, Wang X. Encapsulation of gold nanoparticles with PHB based on coffee ring effect. RSC Adv 2015;5:18501.
[169] Norris DJ, Arlinghaus EG, Meng L, Heiny R, Scriven LE. Opaline photonic crystals: how does self-assembly work? Adv Mater 2004;16:1393–9.
[170] Zhang J, Sun Z, Yang B. Self-assembly of Photonic Crystals from polymer colloids. Curr Opin Colloid Interface Sci 2009;14:103–14.
[171] Choi S, Stassi S, Pisano AP, Zohdi TI. Coffee-ring effect-based three dimensional patterning of micro/nanoparticle assembly with a single droplet. Langmuir 2010;26:11690–8.
[172] Malfatti L, Tokudome Y, Okada K, Yagi S, Takahashi M, Innocenzi P. Coffee stain–driven self-assembly of mesoporous rings. Microporous Mesoporous Mater 2012;163:356–62.
[173] Mu J, Lin P, Xia Q. Concentric rings of polystyrene and titanium dioxide nanoparticles patterned by alternating current signal guided coffee ring effect. Appl Phys Lett 2014;104:261601.
[174] Li Y, Lan L, Xiao P, Sun S, Lin Z, Song W. et al. Coffee-Ring defined short channels for inkjet-printed metal oxide thin-film transistors. ACS Appl Mater Interfaces 2016;8:19643–8.
[175] Zhang Z, Zhang X, Xin Z, Deng M, Wen Y, Song Y. Controlled inkjetting of a conductive pattern of silver nanoparticles based on the coffee-ring effect. Adv Mater 2013;25:6714–8.
[176] Zhang Z, Zhu W. Controllable fabrication of a flexible transparent metallic grid conductor based on the coffee ring effect. J Mater Chem C 2014;2:9587–91.
[177] Bromberg V, Ma S, Singler TJ. High-resolution inkjet printing of electrically conducting lines of silver nanoparticles by edge-enhanced twin-line deposition. Appl Phys Lett 2013;102:214101.
[178] Ma S, Liu L, Bromberg V, Singler TJ. Fabrication of highly electrically conducting fine patterns via substrate-independent inkjet printing of mussel-inspired organic nano-material. J Mater Chem C 2014;2:3885–9.
[179] Layani M, Gruchko M, Milo O, Balberg I, Azulay D, Magdassi S. Transparent conductive coatings by printing coffee ring arrays obtained at room temperature. ACS Nano 2009;3:3537–42.

[180] Dinh NT, Sowade E, Blaudeck T, Hermann S, Rodriguez RD, Zahn DRT. et al. High-resolution inkjet printing of conductive carbon nanotube twin lines utilizing evaporation-driven self-assembly. Carbon 2016;96:382–93.
[181] Khapli S, Rianasari I, Sharma S, Blanton T. Jagannathan, R. Fabrication of hierarchically structured porous films of metal oxides and carbonates through coffee ring effect. Mater Today Proc 2016;3:362–8.
[182] Khapli S, Rianasari I, Blanton T, Weston J, Gilardetti R, Neiva R. et al. Fabrication of hierarchically porous materials and nanowires through coffee ring effect. ACS Appl Mater Interfaces 2014;6:20643–53.
[183] Chung S, Karim MHU, Spencer M, Kwon HJ, Grigoropoulos CP, Alon E. et al. Exploitation of the coffee-ring effect to realize mechanically enhanced inkjet-printed microelectromechanical relays with U-bar-shaped cantilevers. Appl Phys Lett 2014;105:261901.
[184] Sun W, Yang F. Evaporation-induced formation of self-organized gradient concentric rings on sub-micron pre-cast PMMA films. Soft Matter 2014;10:4451.
[185] Lin ZQ, Granick S. Patterns formed by droplet evaporation from a restricted geometry. J Am Chem Soc 2005;127:2816.
[186] Hong SW, Xu J, Xia J, Lin Z, Qiu F, Yang Y. Drying mediated pattern formation in a capillary-held organometallic polymer solution. Chem Mater 2005;17:6223.
[187] Xu J, Xia J, Hong SW, Lin Z, Qiu F, 2 Yang Y. Self-assembly of gradient concentric rings via solvent evaporation from a capillary bridge. Phys Rev Lett 2006;96:066104.